UNIVERSITY OF LATVIA

FACULTY OF PHYSICS, MATHEMATICS AND OPTOMETRY

Guna Krieķe

ERBIUM UPCONVERSION LUMINESCENCE IN TRANSPARENT GLASS CERAMICS CONTAINING TERNARY FLUORIDE NANOCRYSTALS

SUMMARY OF DOCTORAL THESIS

Submitted for the degree of Doctor of Physics
Subfield of Material Physics

Riga, 2020

The doctoral thesis was carried out at the Institute of Solid State Physics, University of Latvia from 2015 to 2020.

The summary of thesis contains an introduction, 3 chapters, conclusions and a reference list.

Type of thesis: scientific paper collection in physics in the subfield of material physics.

Supervisor: *Dr. phys.* **Anatolijs Sarakovskis**, professor, University of Latvia.

Reviewers:
1. *Dr. phys.* **Pavels Onufrijevs**, leading researcher, Riga Technical university;
2. *Dr. habil. phys.* **Ruvins Ferbers**, professor, University of Latvia;
3. *Dr. habil. phys.* **Marina Popova**, professor, Russian Academy of Sciences.

The thesis will be defended at the public session of the Doctoral Committee of Physics, Astronomy and Mechanics, University of Latvia at 15:00 on 4th of December, 2020 in Institute of Solid State Physics, University of Latvia, 8 Kengaraga street, Riga.

The thesis and its summary is available at the Library of the University of Latvia, Kalpaka blvd. 4, Riga.

Chairman of the Doctoral Committee _____

Dr. habil. phys. **Linards Skuja**

Secretary of the Doctoral Committee _____

Annija Sturmane

ABSTRACT

In this research novel transparent Er^{3+} doped glass ceramics containing $NaREF_4$ ($NaLaF_4$, $Na(Gd,Lu)F_4$, $NaYF_4$, $NaErF_4$) and $Ba_4RE_3F_{17}$ ($Ba_4Gd_3F_{17}$, $Ba_4Y_3F_{17}$, $Ba_4Yb_3F_{17}$, $Ba_4Lu_3F_{17}$) nanocrystals were successfully prepared from melt-quenched glasses.

The crystallization and spectroscopic properties of precursor glass and glass ceramics were analysed. The enhancement of upconversion luminescence intensity of the investigated glass ceramics up to two orders of magnitude in comparison to the precursor glasses was achieved and attributed to incorporation of Er^{3+} ions in the fluoride nanocrystals.

In $NaREF_4:Er^{3+}$ containing glass ceramics two polymorphic modifications – cubic $NaREF_4$ and hexagonal $NaREF_4$ – were prepared by variation of chemical composition and temperature of heat treatment. In $Ba_4RE_3F_{17}$: Er^{3+} containing glass ceramics thermal analysis and microscopy studies suggested ordering of $Ba_4RE_3F_{17}$ structure during the heat treatment. The changes in the crystalline structure was analysed using time-resolved site-selective spectroscopy, which confirmed order-disorder phase transition from metastable cubic to rhombohedrally distorted cubic $Ba_4RE_3F_{17}$ phase.

TABLE OF CONTENTS

1. INTRODUCTION

1.1. Motivation

Transparent oxyfluoride glass ceramics are composites typically consisting of fluoride nanocrystals dispersed in oxide glass matrix. The low phonon energy of the fluoride phase combined with transparency, good chemical and mechanical properties of oxide glass matrix make these materials suitable for optical applications [1], [2].

Among other rare earth (RE) ions, erbium (Er^{3+}) is a widely investigated candidate for infrared to visible upconversion luminescence (UCL). The efficiency of this process depends mainly on Er^{3+} distribution and properties of host matrix [3]. Among other hosts, RE^{3+} containing fluorides exhibit good Er^{3+} solubility and low phonon energy, which improves UCL efficiency. In this research two types of thernary fluorides which exhibit all requirements for efficient UCL – hexagonal $NaREF_4$ ($NaLaF_4$, $Na(Gd,Lu)F_4$, $NaYF_4$, $NaErF_4$) and rhombohedral $Ba_4RE_3F_{17}$ ($Ba_4Gd_3F_{17}$, $Ba_4Y_3F_{17}$, $Ba_4Yb_3F_{17}$, $Ba_4Lu_3F_{17}$) – were prepared in glass ceramics and analysed in detail.

The main motivation of this research is the development of new efficient material for UCL: Er^{3+} doped transparent glass ceramics. Prior to this research hexagonal $NaREF_4$ was successfully prepared only in La^{3+} and Gd^{3+} containing systems [4], [5] and no information was available about formation of $Ba_4RE_3F_{17}$ in glass ceramics.

1.2. Main objective and tasks

The main objectives of this thesis are preparation, characterization and analysis of upconversion processes in transparent erbium doped glass ceramics containing sodium rare earth fluorides and barium rare earth fluorides. Following tasks were performed:
1. Synthesis of oxyfluoride glasses using melt-quenching method;
2. Characterization of crystallization processes in the precursor glasses;
3. Preparation of glass ceramics containing β-$NaREF_4$ and $Ba_4RE_3F_{17}$ nanocrystals;
4. Analysis of dominant upconversion luminescence processes in glass ceramics.

1.3. Scientific novelty

In this research novel transparent glass ceramics containing cubic $NaLaF_4$, hexagonal $NaYF_4$, $NaErF_4$ and $Na(Gd,Lu)F_4$ solid solutions, cubic

and rhombohedral $Ba_4RE_3F_{17}$ ($Ba_4Gd_3F_{17}$, $Ba_4Y_3F_{17}$, $Ba_4Yb_3F_{17}$, $Ba_4Lu_3F_{17}$), tetragonally distorted cubic $NaF-BaF_2-YF_3$ and $NaF-BaF_2-YbF_3$ nanocrystals has been prepared.

Time-resolved site-selective spectroscopy was successfully used to analyse phase formation, activator local environment and activator distribution in glass and crystalline phase. External standard method for quantitative characterization of Er^{3+} content in crystalline phase was proposed.

Incorporation efficiency of RE^{3+} ions in the crystalline phase of glass ceramics was analysed and was found to improve with the increase of RE^{3+} ionic radius.

1.4. List of publications included in thesis

1. G. Krieke, A. Antuzevics, M. Springis, U. Rogulis, Upconversion luminescence in transparent oxyfluoride glass ceramics containing hexagonal $NaErF_4$, J. Alloys Compd. 798 (2019) 326–332.
2. G. Krieke, A. Sarakovskis, M. Springis, Cubic and rhombohedral $Ba_4Lu_3F_{17}$:Er^{3+} in transparent glass ceramics: Crystallization and upconversion luminescence, J. Lumin. 200 (2018) 265–273.
3. G. Krieke, A. Sarakovskis, M. Springis, Ordering of fluorite-type phases in erbium-doped oxyfluoride glass ceramics, J. Eur. Ceram. Soc. 38 (2018).
4. G. Krieke, A. Sarakovskis, M. Springis, Upconversion luminescence of Er^{3+}/Yb^{3+} and their role in the stabilization of cubic $NaLaF_4$ nanocrystals in transparent oxyfluoride glass ceramics, J. Non. Cryst. Solids. (2018).
5. G. Krieke, A. Sarakovskis, R. Ignatans, J. Gabrusenoks, Phase transitions and upconversion luminescence in oxyfluoride glass ceramics containing $Ba_4Gd_3F_{17}$ nanocrystals, J. Eur. Ceram. Soc. 37 (2017).
6. G. Krieke, A. Sarakovskis, M. Springis, Upconversion luminescence of a transparent glass ceramics with hexagonal $Na(Gd,Lu)F_4$ nanocrystals, J. Alloys Compd. 694 (2017) 952–958.
7. G. Krieke, A. Sarakovskis, Crystallization and upconversion luminescence of distorted fluorite nanocrystals in Ba^{2+} containing oxyfluoride glass ceramics, J. Eur. Ceram. Soc. 36 (2016) 1715–1722.
8. A. Sarakovskis, G. Krieke, Upconversion luminescence in erbium doped transparent oxyfluoride glass ceramics containing hexagonal $NaYF_4$ nanocrystals, J. Eur. Ceram. Soc. 35 (2015).

1.5. List of conference presentations

1. G. Krieķe, M. Spriņģis, A. Sarakovskis, Augšuppārveidotā luminiscence nātrija retzemju fluorīdus saturošā oksifluorīdu stikla keramikā, 77th UL Scientific Conference, March 29, 2019, Riga, Latvia

2. G. Krieķe, A. Antuzevics, M. Spriņģis, U. Rogulis, Augšuppārveidotā luminiscence β-NaErF₄ saturošā stikla keramikā, 35th ISSP UL Scientific Conference, February 20–22, 2019, Riga, Latvia.

3. G. Krieke, A. Sarakovskis, M. Springis, Ordering of fluorite-type phases in oxyfluoride glass ceramics: crystallization and upconversion luminescence Cost Action: TD1401 (FAST) annual meeting, March 8–9, 2018, Bucharest, Romania.

4. Guna Krieke, Kristalizācija un erbija jonu luminiscence oksifluorīdu stikla keramikās, 76th UL Scientific Conference, April 13, 2018, Riga, Latvia.

5. G. Krieke, A. Sarakovskis, M. Spriņģis, Kristalizācija un erbija jonu luminiscence Ba₄Lu₃F₁₇ saturošā stikla keramikā, 34th ISSP UL Scientific Conference, February 20–22, 2018, Riga, Latvia.

6. G. Krieke, A. Sarakovskis, R. Ignatans, J. Gabrusenoks, Phase transition of Ba₄Gd₃F₁₇ nanocrystals in Er³⁺ doped transparent glass ceramics 15th Conference & Exhibition of the European Ceramic Society, July 9–13, 2017, Budapest, Hungary.

7. G. Krieķe, A. Sarakovskis, NaLaF₄ kristalizācija ar erbija un iterbija joniem aktivētā stikla oksifluorīdu keramikā, 33th ISSP UL Scientific Conference, February 22–24, 2017, Riga, Latvia.

8. G. Krieke, A. Sarakovskis, M. Springis, The upconversion luminescence of erbium doped glass ceramics with β-NaYF₄ nanocrystals, International Congress on Ceramics, August 21–25, 2016, Dresden, Germany.

9. G. Krieķe, A. Sarakovskis, Erbija jonu augšuppārveidotā luminiscence bāriju saturošā oksifluorīdu stikla keramikā, 32th ISSP UL Scientific Conference, February 17–19, 2016, Riga, Latvia.

1.6. Author's contribution

All research presented in the work was performed in Institute of Solid State Physics, University of Latvia. The author realized the synthesis of materials and most of the characterization including differential thermal analysis (DTA), X-ray diffraction (XRD), scanning electron microscopy (SEM) and optical spectroscopy measurements. Transmission electron microscopy (TEM) analysis was performed by Krisjanis Smits. Rietveld refinement of $Ba_4Gd_3F_{17}$ and $Ba_4Lu_3F_{17}$ microcrystalline samples was performed by Reinis Ignatans. Raman spectra of cubic and rhombohedral $Ba_4Gd_3F_{17}$ were measured by Jevgenijs Gabrusenoks. The non-radiative relaxation rates in β-NaErF₄ containing glass ceramics were calculated by Maris Springis. The analysis of the data was performed by the author with the collaboration of all co-authors of the scientific papers.

2. LITERATURE REVIEW

2.1. Upconversion luminescence

Upconversion luminescence (UCL) is an anti-Stokes process, in which photons with low energy are converted in high energy photons [6]. UCL materials have been extensively studied for various perspective optical applications such as UCL lasers [7], [8], three-dimensional displays [9], [10], optical memory devices [11], [12], optical switches [13], solar harvesting [14], optical sensors [15], [16], actuators [17] and biomedical probes [18], [19].

Four main mechanisms for UCL has been proposed: multistep excitation due to excited state absorption, energy transfer upconversion, cooperative upconversion between two or three ions and photon avalanche upconversion [6]. These mechanisms are schematically represented in Fig. 2.1.
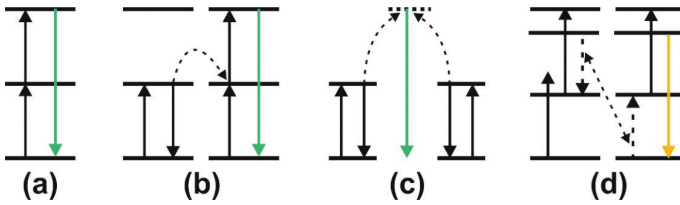

Fig. 2.1. UCL mechanisms: a) excited state absorption, b) energy transfer UCL, c) cooperative UCL, d) photon avalanche UCL.

In case of excited state absorption two or more photons are sequentially absorbed by a single activator ion (see Fig. 2.1. a).

Energy transfer UCL occurs by absorption of photons by two or more activator ions followed by energy transfer from one excited ion to another which promote one of the activator ions to higher emitting state (see Fig. 2.1. b). The efficiency of this process depends on the distances between activator ions which is mainly determined by their content in the UCL material [20].

In case of cooperative UCL the photons are absorbed by two activator ions. Both of these ions decay simultaneously and either emit single photon with doubled energy or excite another ion to excited state resonant with the doubled excitation energy (See Fig. 2.1. c) [21].

The photon avalanche UCL is relatively uncommon type of UCL in which cross-relaxation induces excited state absorption (See Fig. 2.1. d). In case of this mechanism, the excitation energy is not resonant with transitions from ground state to excited states but it matches with transitions between some of the excited states. The non-resonant excitation of intermediate state

enables excited state absorption and cross-relaxation from the emitting state non-linearly increase the population of the intermediate state. The theoretical models indicate that photon avalanche UCL can occur when cross-relaxation rate is higher than radiative and other non-radiative relaxation rates of excited states [22].

The UCL mechanisms can be distinguished by analysis of luminescence and luminescence excitation spectra, luminescence kinetics and excitation power dependence on luminescence intensity [6]. The highest UCL efficiency has been obtained for energy transfer UCL which typically exhibit several orders of magnitude higher UCL intensity than other mechanisms [6].

2.2. Requirements for efficient upconversion luminescence

The efficiency of the UCL processes depends on the properties of the activator and host matrix.

Trivalent RE ions are considered to be suitable activators for the UCL due to multiple excited states with long lifetimes and similar energy gaps between them [3]. The highest UCL efficiency has been achieved in erbium ion (Er^{3+}) doped materials due to equally spaced energy levels of Er^{3+}, which enable efficient near-infrared (NIR) to visible UCL [23]. Often Er^{3+} doped materials are co-doped with Yb^{3+} as a sensitizer with large absorption cross-section, which improves NIR absorption, therefore enhancing UCL [24].

Typical UCL hosts include oxides, halides and chalcogenides. The main requirements for the host matrix include low phonon energy of matrix, low local symmetry and good solubility of the activator ion. Significant attention has been focused on the fluoride hosts due to relatively good thermal and chemical stability combined with sufficiently low phonon energy, which reduces the non-radiative relaxation rate [24]. The local symmetry of RE^{3+} activator determines the transition probabilities of partly forbidden f-f transitions. Typically, RE^{3+} positions without inversion symmetry are required to enhance transition probabilities [3].

In addition, good RE^{3+} solubility in the host matrix is required. It can be realized by matching the ionic radii of the host matrix and RE^{3+} ions. RE^{3+} solubility can be realized by homovalent substitution in RE^{3+} containing compounds such as REF_3 and $AREF_4$ (A=Li-K), however, RE^{3+} can be also incorporated in compounds, where they require heterovalent substitution, such as MF_2 (M=Ca-Ba), which form MF_2-REF_3 solid solutions [25].

This research is devoted to investigation of the UCL processes in ternary $NaREF_4$ and $Ba_4RE_3F_{17}$ containing composites, which satisfies all requirements for efficient UCL.

2.3. NaREF$_4$ as a host for upconversion luminescence

NaREF$_4$ compounds are considered to be the most efficient fluoride hosts for UCL [23], [26].

Two polymorphic modifications of NaREF$_4$ are known: low temperature hexagonal β-NaREF$_4$ (space group P$\bar{6}$) and high temperature cubic α-NaREF$_4$ with fluorite structure (space group Fm$\bar{3}$m). β-NaREF$_4$ can be prepared in all NaREF$_4$ systems (La-Lu) and α-NaREF$_4$ modification can be prepared for all RE except for La and Ce. The latter compound forms solid solutions with variable NaF-REF$_3$ ratio [27]. Unit cells of α-NaREF$_4$ and β-NaREF$_4$ are shown in Fig. 2.2.
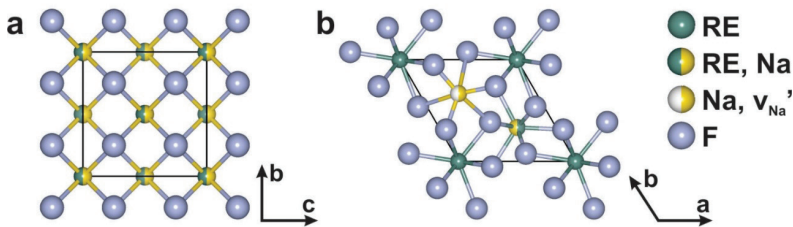

Fig. 2.2. Crystal structure of a) α-NaREF$_4$ and b) β-NaREF$_4$. Atomic positions taken from [28], [29].

In structure model of α-NaREF$_4$ reported in [28], all cationic positions are randomly filled with Na$^+$ and RE^{3+} ions and the site symmetry is cubic (O$_h$). In β-NaREF$_4$ there are three cationic positions: first is filled with RE^{3+} ions (C$_{3h}$), second is filled with RE^{3+} and Na$^+$ (C$_{3h}$) and third is half-filled with Na$^+$ and vacancies (C$_3$) [29]. According to the crystal structure models of NaREF$_4$, β-NaREF$_4$ exhibits RE^{3+} positions with lower symmetry, which improves the transition probabilities of activator ions. However, the experimental investigations of local environment of doped NaREF$_4$ crystals revealed that local symmetry of RE^{3+} positions in both phases are lower than expected [30], [31]. In addition, the phonon energy of these polymorphs is low (<500 cm^{-1}) [32], [33], therefore, both α-NaREF$_4$ and β-NaREF$_4$ can be expected to exhibit good UCL properties. Nevertheless, UCL efficiency in the hexagonal phase is detected to be approximately order of magnitude higher in comparison to cubic polymorph [34]. This effect has been attributed to broader distribution of phonon modes in cubic phase due to random distribution of cations in the crystalline structure [35].

Despite superior UCL properties of β-NaREF$_4$, its applications in optics are limited, because the growth of large β-NaREF$_4$ are difficult due to incongruent melting and phase transition to high temperature polymorph, therefore single crystals can only be prepared from non-stoichiometric melts [36].

2.4. Barium rare earth fluorides

Cubic MF_2: RE^{3+} (M=Ca-Ba) with fluorite structure are common hosts for optical applications. Despite heterovalent substitution required for incorporation of RE^{3+} ions in M^{2+} position, MF_2 compounds form wide regions of solid solutions with all RE^{3+} ions. Unfortunately, in MF_2 structure RE^{3+} ions tend to form clusters, which result in cross-relaxation between RE^{3+} ions. In BaF_2 single crystals clustering of Er^{3+} ions was detected in samples doped with as low Er^{3+} content as 0.05 mol% [37]. The cross-relaxation processes in these materials can be reduced by incorporation of other RE^{3+} ions such as La, Y, Lu, which act as spacers between activator ions.

Among all MF_2 compounds, BaF_2 is the most promising host for optical applications due to lower phonon energy (346 cm^{-1}) than CaF_2 (484 cm^{-1}) and SrF_2 (397 cm^{-1}) [38], [39], therefore in this research Er^{3+} doped BaF_2-REF_3 phases are investigated.

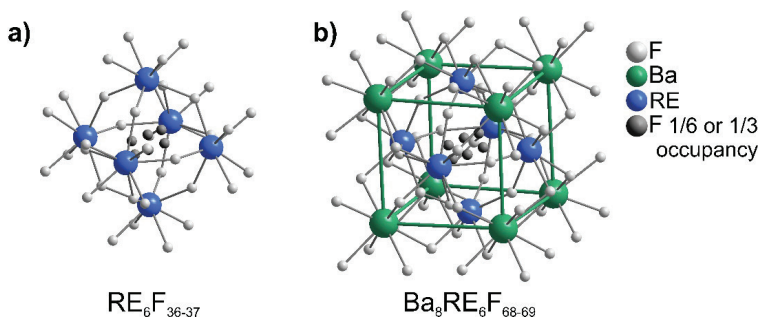**Fig. 2.3. Typical clusters in BaF_2-REF_3 systems [40].**

In BaF_2 typically octahedral RE_6F_{36-37} clusters are formed (see Fig. 2.3. a). These clusters are surrounded by eight Ba^{2+} ions, thus forming rare earth octahedral superclusters $Ba_8[RE_6F_{68-69}]$ (see Fig. 2.3. b) [37]. The superclusters are structurally similar to BaF_2 unit cell and they can be incorporated in the BaF_2 without considerable distortion of fluorite structure, which explains the formation of wide regions of solid solutions in BaF_2-REF_3 system. Special case of BaF_2-REF_3 compounds is associated with chemical composition $Ba_4RE_3F_{17}$ (RE=Sm-Lu). Two polymorphic modifications of $Ba_4RE_3F_{17}$ can be prepared: metastable cubic $Ba_4RE_3F_{17}$ with fluorite structure and rhombohedrally distorted cubic $Ba_4RE_3F_{17}$ [41]. The structure of this compound consists only from $Ba_8[RE_6F_{68-69}]$ superclusters witch are strictly ordered in rhombohedral phase and are randomly orientated in relation to one and another in cubic phase [42].

Schematic representation of supercluster distribution in cubic and rhombohedral $Ba_4RE_3F_{17}$ is shown in Fig. 2.4.

a) Metastable cubic $Ba_4RE_3F_{17}$
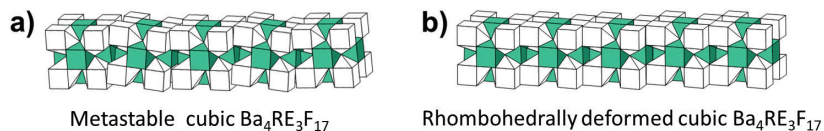
b) Rhombohedrally deformed cubic $Ba_4RE_3F_{17}$

Fig. 2.4. Schematic representation of supercluster distribution in a) metastable cubic and b) rhombohedrally deformed cubic $Ba_4RE_3F_{17}$.

Recently $Ba_4RE_3F_{17}$ compounds were proven to be excellent hosts for UCL [43]. Similarly to β-NaREF$_4$, $Ba_4RE_3F_{17}$ exhibit incongruent melting [44], which restricts the use of this fluoride.

2.5. Transparent oxyfluoride glass ceramics

Both β-NaREF$_4$ and $Ba_4RE_3F_{17}$ can be expected to be suitable hosts for UCL, but the growth of large single crystals is difficult for these ternary compounds, thus the use of β-NaREF$_4$ and $Ba_4RE_3F_{17}$ in optics is limited especially in applications where transparency is required. This drawback can be overcome by preparation of transparent nanocrystalline composites.

One of the suitable classes of materials are oxyfluoride glass ceramics – composite materials consisting of fluoride nanocrystals homogeneously dispersed in oxide glass matrix. Oxyfluoride glass ceramics combine the best properties of oxide glasses and fluoride crystals, such as good chemical and mechanical properties of glasses with superior spectroscopic properties of fluoride crystals. In addition, with careful control of size of crystals it is possible to prepare transparent composites.

The size of nanocrystals affects the spectroscopic properties of these nanocomposites. In larger crystals the luminescence quenching on the surface of the crystals is reduced, therefore improving UCL efficiency, nevertheless, nanocrystals larger than 50–100 nm cause light scattering, therefore, the optimal heat treatment conditions are crucial for the preparation of transparent glass ceramics with satisfactory spectroscopic properties [45]. Photographs of precursor glass and glass ceramics heat treated at different temperatures are shown in Fig. 2.5.
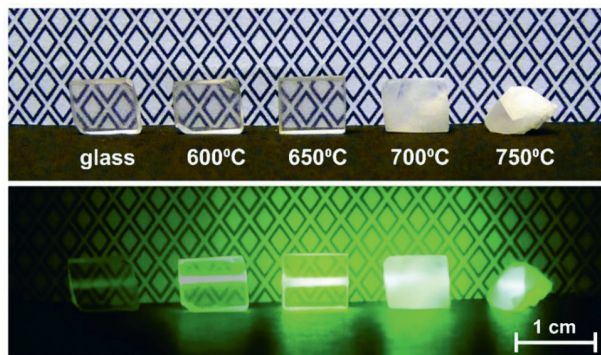
Fig. 2.5. Photograph of Er³⁺ doped precursor glass and oxyfluoride glass ceramics under ambient light (upper row) and excited with 975 nm laser (lower row) [46].

Wide variety of simple and complex fluoride phases can be prepared in oxyfluoride glass ceramics including alkaline earth fluorides (MF_2, M=Mg-Ba), rare earth fluoride (REF_3 where RE=La-Lu), several alkali rare earth fluorides ($LiYF_4$, $NaREF_4$, KRE_xF_{3x+1}) and fluorite type MF-REF_3 solid solutions [1], [47]. Despite excellent spectroscopic properties of β-$NaREF_4$, most of the efforts prior to these thesis were devoted to investigation of α-$NaREF_4$ containing glass ceramics and hexagonal phase was successfully prepared in $NaLaF_4$ and $NaGdF_4$ systems only [48], [49]. Among MF_2-REF_3 phases in glass ceramics no distorted fluorite type phases were identified previously. Therefore, in this research novel glass compositions, in which β-$NaREF_4$ and $Ba_4RE_3F_{17}$ phases could be formed, were developed and characterized.

2.6. Synthesis methods of oxyfluoride glass ceramics

Typically, oxyfluoride glass ceramics are prepared using melt quenching or sol-gel synthesis and subsequent heat treatment, which promotes formation of fluoride nanocrystals.

The melt quenching method consists of melting of precursors and rapid cooling of the glass melt. The glass ceramics are prepared by heat treatment of precursor glasses. The size, shape and concentration of crystals depends on nucleation and growth rate which is determined by heat treatment parameters and chemical composition of precursor glass. There are two main drawbacks of melt quenching method: changes in the chemical composition during the melting of oxyfluoride glasses and liquid-liquid phase separation [1].

The melt quenching of oxyfluoride glasses is usually performed in air. At high temperatures fluoride compounds are not stable and can decompose, react with moisture or evaporate from the melt [50]–[52] resulting in changes of the chemical composition of glass. The fluorine loss during the melting

depends on the chemical composition and melting conditions of glass and can be up to 50 mol% [53].

Due to limited solubility of oxides and fluorides, often phase separation is detected in melt quenched oxyfluoride glasses, which can increase light scattering [54]. However, nanosized phase separation droplets can act as nucleation centres in crystallization of transparent oxyfluoride glass ceramics [55]. The microstructure of melt quenched precursor glass and glass ceramics containing $NaLaF_4$ nanocrystals is shown in Fig. 2.6.
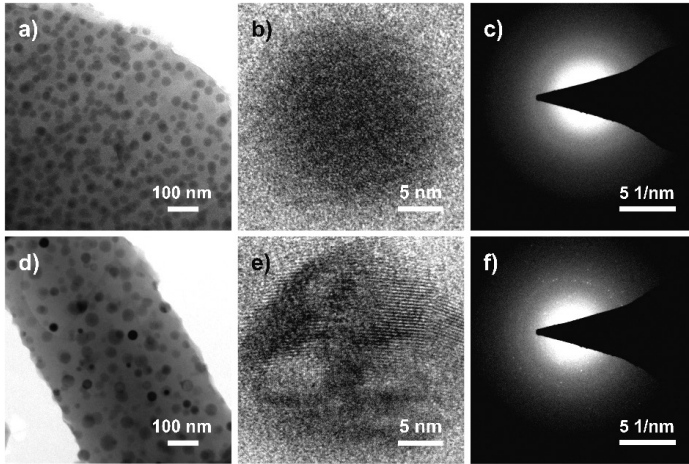

Fig. 2.6. (a, b, d, e) TEM micrographs and (c, f) electron diffraction patterns of (a–c) melt quenched oxyfluoride precursor glass and (d–f) glass ceramics containing $NaLaF_4$ nanocrystals [56].

Both glass and glass ceramics consist of similar spherical particles dispersed in glass matrix, however, high resolution micrographs (Fig. 2.6. b and e) and electron diffraction patterns (Fig. 2.6. c and f) indicate that the particles are amorphous in precursor glass and crystalline in glass ceramics.

The melt quenching method is suitable for preparation of bulk materials, however the precise control of chemical composition of precursors and melting conditions is required to obtain reproducible results.

An alternative approach for preparation of oxyfluoride glass ceramics is sol-gel method. It is solution-based method which consists of hydrolysis and polycondensation of metal organic compounds or salts followed by drying and heat treatment of precursor gels [57]. The main advantage of sol-gel process is the reduction of temperature of heat treatment, thus significantly reducing fluorine loss in glass. In addition, glass ceramic compositions which cannot be made using melt quenching method can be prepared using this method, such as glass ceramics with high SiO_2 content [1]. However, it is often difficult

to prevent the presence of organic impurities and hydroxyl groups which are detrimental for spectroscopic properties of glass ceramics [45], [58].

The sol-gel process is suitable for preparation of coatings and thin films but it is inconvenient for preparation of the bulk materials, because the precursor gels are prone to cracking during the drying [59].

In this research melt quenching method is used for preparation of glass ceramic. To prevent considerable fluorine loss, the glasses are melted in covered crucibles using rapid heating rate and short melting time (30 min). Large scale phase separation is prevented by adjusting the fluorine content in precursor glass.

2.7. Characterization of oxyfluoride glass ceramics

For quantitative analysis of chemical composition of precursor glasses traditionally wet chemical methods are used [60], which can be adapted for oxyfluoride glasses, including the determination of fluorine content [61]. These methods are destructive, therefore other methods such as X-ray fluorescence and X-ray photoelectron spectrometry are often preferred [62], [63].

The characteristic temperatures, such as glass transition and crystallization of glasses are commonly determined from differential thermal analysis or differential scanning calorimetry data. These methods can also be used for determination of crystallization mechanism, activation energy and the shape of crystals [64].

For identification of crystalline phases mainly X-ray diffraction is used. It can also be used for estimation of crystallite size [65] and the crystalline fraction [66]. Due to multicomponent nature, many compounds with similar structures can form of oxyfluoride glass ceramics, therefore the phase identification should not be based solely on X-ray diffraction data [1].

Electron microscopy is an informative method for direct observation of crystalline phase size and morphology which is indispensable tool for studying of crystallization processes in glass [67]. An example of morphology alteration during the crystallization of oxyfluoride glass is shown in Fig. 2.7.
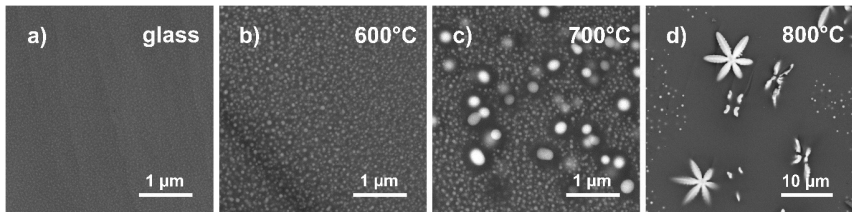

Fig. 2.7. SEM micrographs of a) phase-separated precursor glass and (f–h) glass ceramics heat treated at 600–800 °C (adapted from [68]).

The changes in the size and shape of particles formed in precursor glass indicate the growth of the crystalline phase. The snowflake-like morphology of crystals formed in glass ceramics heat treated at 800 °C is associated with the formation of hexagonal LaF_3 [68].

Typical spectroscopic characterization methods of oxyfluoride glass ceramics include vibration spectroscopy methods (infrared and Raman spectrometry), absorption spectroscopy and luminescence spectroscopy.

The vibration spectrometry methods are widely used to analyse the structure and bonding in glasses [69]. These methods have been also successfully used to identify the crystalline phases and estimate the size of nanocrystals in oxyfluoride glass ceramics [70], [71].

Absorption spectrometry methods are useful for identification of impurities, determination optical losses and calculation of absorption cross-section [72]. The absorption data can be used for Judd-Ofelt theory calculations which have been employed in glass ceramics for determination of oscillator strength, radiative transition probabilities and branching ratios of activator ions [73].

Luminescence spectroscopy is used for characterization of various spectroscopic properties such as luminescence quantum efficiency, lifetime of emitting states, dynamics of radiative and non-radiative relaxations [72]. The spectroscopic properties of activator ions is influenced by the host matric, therefore the activator ions can be used as probes to detect point defects, their aggregates and activator local environment [74], [75]. In oxyfluoride glass ceramics the changes in the spectroscopic properties such as lifetimes of emitting states and changes in luminescence band linewidths have been successfully used to analyse the crystallization processes [76], [77].

The comparison of luminescence excitation and luminescence spectra of Er^{3+} ions in glass and crystalline phase of $NaLaF_4$ containing glass ceramics is shown in Fig. 2.8.
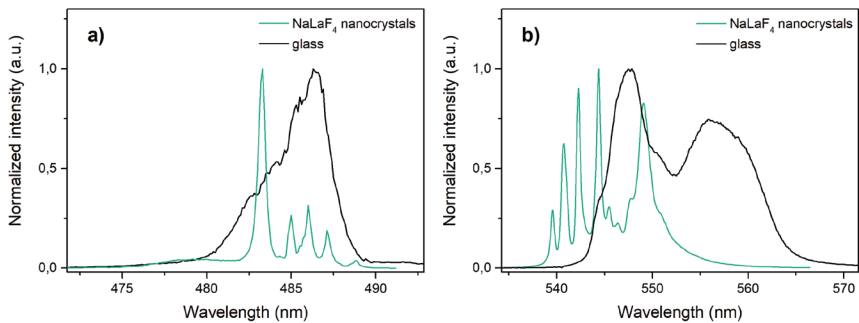

Fig. 2.8. a) luminescence excitation and b) luminescence spectra of Er^{3+} ions in amorphous and crystalline phase of $NaLaF_4$ containing glass ceramics (adapted from [68]).

Broad Er^{3+} luminescence excitation and luminescence bands can be detected in the amorphous phase due to random distribution of Er^{3+} ions in glass network, however, in crystalline phase sharp and narrow luminescence bands are observed which are attributed to strictly ordered Er^{3+} positions in $NaLaF_4$ lattice [68]. As the result, the analysis of luminescence spectra of glass ceramics can offer invaluable information about distribution of activator ions, however one of the greatest challenges of oxyfluoride glass ceramics is the quantitative determination of activator distribution in crystalline and glass phase.

2.8. Rare earth ion distribution in oxyfluoride glass ceramics

In oxyfluoride glass ceramics rare earth activator ions can be located in both glass and crystalline phase. The chemical analysis of phase separated oxyfluoride melts using mass spectrometry have revealed strong tendency for RE^{3+} ions to incorporate in fluoride-rich phases [78] and similar trend have been detected in oxyfluoride glass ceramics. An example of element distribution in glassy phase and $Ba_4Y_3F_{17}$ nanocrystal of oxyfluoride glass ceramics is shown in Fig. 2.9.

In oxyfluoride glass ceramics several approaches for determination of RE ion distribution have been proposed in literature. The chemical composition has been estimated from energy dispersive X-ray spectroscopy data [80], [81], chemical analysis of nanocrystlals, dissolved from glass matrix [82], XRD data [83], electron paramagnetic resonance data [76], absorption spectra [84], luminescence decay [85] and luminescence excitation spectra [86]. The highest precision can be obtained from XRD and chemical analysis of nanocrystals. However, these methods are not applicable for all oxyfluoride glass ceramics. The analysis of interplannar distances from XRD data cannot be used for materials with small deviations in ionic radii of activator and host, such as $NaYF_4$: Er^{3+} and the chemical dissolution can cause the precipitation of RE fluorides formed from RE^{3+} ions in oxide glass matrix which results in deviations in chemical composition.
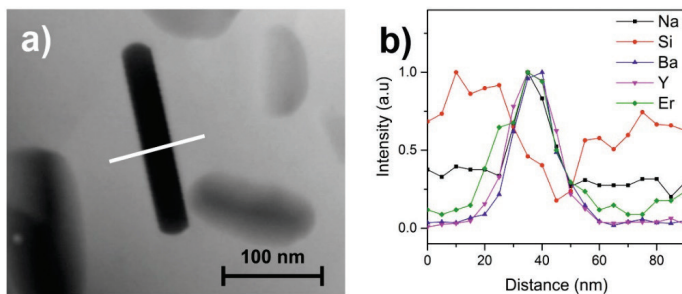

Fig. 2.9. a) TEM micrograph and b) element distribution in Er^{3+} doped oxyfluoride glass and $Ba_4Y_3F_{17}$ nanocrystal (adapted form [79], white line indicate the scanned region).

The activator content in the crystalline phase is a crucial factor for efficient UCL. In Er^{3+} doped materials the relative intensity of luminescence bands and lifetime of emitting states depends on Er^{3+} content [87]. This effect can be used for quantitative determination of Er^{3+} content. In this research external standard method based on the comparison of spectroscopic properties of Er^{3+} ions in glass ceramics with Er^{3+} doped microcrystalline samples is proposed.

2.9. Applications of transparent oxyfluoride glass ceramics

The excellent luminescence efficiency and good transparency of oxyfluoride glass ceramics enables the use of these nanomaterials for many applications in optics.

Currently oxyfluoride glass ceramics are commercially available as transparent visualizers for infrared laser detection [88], [89], but, these materials have also been extensively investigated for various uses in sensors and photonic devices.

Due to intrinsic characteristics of glass matrix, the oxyfluoride glass ceramics can be prepared as fibres which exhibit superior luminescence efficiency in comparison to precursor glasses and are perspective materials for fibre lasers and amplifiers [90], [91]. The precursor glasses can also be selectively crystallized using laser patterning which have proven to be suitable for preparation of optical gratings and waveguides [92]. In oxyfluoride glasses both randomly oriented crystallized regions [93] and highly ordered single crystals [94] have be formed using this method.

Recently significant attention has been devoted to investigation of glass ceramics for application in optical thermometry. Many variations of optical temperature sensors exist; however, best results have been achieved for sensors based on the measurements of luminescence lifetime or luminescence intensity ratio of thermally coupled emitting states. Among others Er^{3+} doped oxyfuoride glass ceramics have been extensively investigated due to thermally induced repopulation of $^2H_{11/2}$ from $^4S_{3/2}$ emitting state which results in variation of luminescence intensity ratio of these emitting states [95].

Oxyfluoride glass ceramics have been investigated as promising scintillator materials for X-ray imaging [96], [97]. Excellent efficiency that surpasses commercial scintillator crystals have been recently detected in $Na_5Gd_9F_{32}:Tb^{3+}$ containing glass ceramics [98]. These materials are prone to formation of radiation defects in glass matrix [99]. For scintillator applications the radiation resistance can be improved by addition of dopant ions [100], however, the defect formation in oxyfluoride glass ceramics have been used to develop erasable high dose radiation dosimeters [101].

Oxyfluoride glass ceramics have been proposed as suitable materials for all-optical solid state cryocooling in which anti-Stokes luminescence is used to cool macroscopic objects [102]. The main advantages include compact

design and high reliability of cryocoolers without vibrations, moving parts or fluid coolants [102] and for now cooling from room temperature up to 91 K have been achieved [94]. Cryocooling have been investigated in Tm^{3+} and Yb^{3+} doped transparent materials including glass ceramics [103], [104].

Considerable effort has been devoted to investigation of glass ceramics for photovoltaic applications. Oxyfluoride glass ceramic coatings can improve the infrared absorption of silicon solar cells by IR to visible UCL [2]. Unfortunately, the increase in efficiency of such solar cells remains less than 2% [105] and it is attributed mainly to the narrow absorption bands and low absorption cross-section of trivalent lanthanide ions [14].

Other potential applications include luminescent materials for white light emitting diodes [106] and UCL lighting devices [107], non-linear transmittance based optical switches [108], three dimensional displays [9] and UCL materials for photo-catalysis [109].

3. MATERIALS AND METHODS

3.1. Material synthesis

The oxyfluoride glass ceramics were prepared from melt quenched oxyfluoride glasses. The precursor glasses with the general composition of Na_2O-NaF-REF_3-Al_2O_3-SiO_2 and Na_2O-BaF_2-REF_3-Al_2O_3-SiO_2 were prepared from high purity oxide, fluoride and carbonate precursors. The glasses were melted in covered corundum crucibles at 1500 °C for 30 min and afterwards casted in stainless steel molds. The oxyfluoride glass ceramics were prepared after isothermal heat treatment of the precursor glasses.

Microcrystalline fluorides were prepared using co-precipitation, hydrothermal synthesis and thermal treatment in F_2/He and Ar atmosphere for comparison of spectroscopic properties.

3.2. Characterization of samples

The thermal properties of precursor glasses were analyzed using differential thermal analysis (DTA). The measurements were carried out in a differential thermal analyzer (Shimadzu Corp. DTG-60) at a heating rate of 10 K/min using Al_2O_3 as a reference.

The crystalline phases in precursors and glass ceramics were determined using X-ray diffraction data obtained by PANalytical X'Pert Pro (Cu K_α tube, 40 kV and 30 mA) and Rigaku MinFlex (Cu K_α tube, 40 kV and 15 mA) diffractometers. The atomic coordinates of $Ba_4RE_3F_{17}$ compounds were calculated with Rietveld analysis using Profex software [110]. Software Vesta was used for visualization of the crystal structure [111].

The microstructure of the glass ceramics was analyzed by scanning electron microscopy (SEM) using Tescan Lyra operated at 15 kV and transmission electron microscopy (TEM) using Tecnai G2 F20 operated at 200 kV.

The Raman spectra were measured using a 1403 double grating Spex-Ramalog spectrophotometer with a conventional photon counting system.

Luminescence was excited by a wavelength tunable pulsed solid state laser Ekspla NT342/3UV and temperature controlled continuous wave (CW) laser diode. The emission signal was detected by Andor DU-401-BV CCD camera coupled to Andor SR-303i-B spectrometer. Luminescence decay was measured using a photomultiplier tube and digital oscilloscope Tektronix TDS 684A. Low temperature measurements were performed using Advanced Research Systems DE202 N cold finger type He cryostat.

4. RESULTS AND DISCUSSION

4.1. Crystallization of NaREF$_4$ containing glass ceramics

In Na$_2$O-NaF-REF$_3$-Al$_2$O$_3$-SiO$_2$ based precursor glasses after appropriate heat treatment β-NaREF$_4$ crystalline phase can be prepared. Typical XRD patterns of precursor and glass and glass ceramics heat treated at 550–700 °C for 2 h is shown in Fig. 4.1.
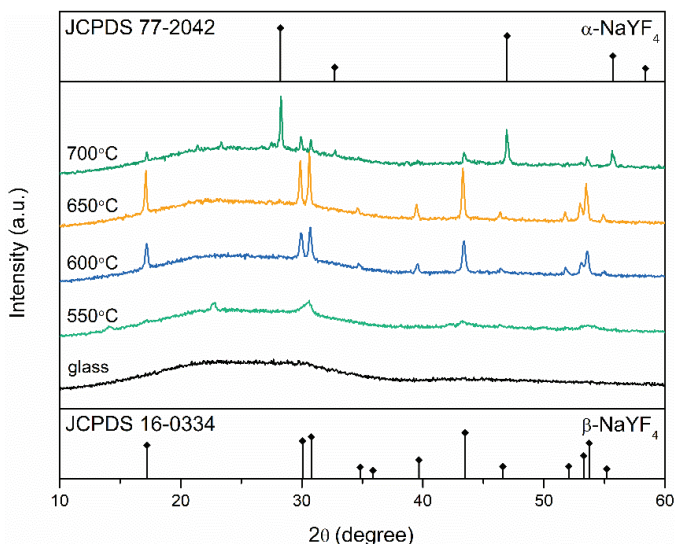

Fig. 4.1. XRD patterns of Na$_2$O-NaF-YF$_3$-Al$_2$O$_3$-SiO$_2$: Er^{3+} precursor glass and glass ceramics heat treated at 550–700 °C for 2 h

The precursor glasses in this system were X-ray amorphous. The thermal treatment of Na$_2$O-NaF-YF$_3$-Al$_2$O$_3$-SiO$_2$: Er^{3+} glass promoted the formation of crystalline phases. Heat treatment at the temperature close to glass transition temperature resulted in the formation of metastable phase with unknown crystalline structure which have been previously observed in melt quenched NaF-YF$_3$ binary system [112]. The increase of the temperature of heat treatment up to 600 °C promoted the formation of β-NaYF$_4$. Heat treatment at temperature higher than the phase transition temperature of β-NaYF$_4$ resulted in the formation of high temperature polymorph – α-NaYF$_4$.

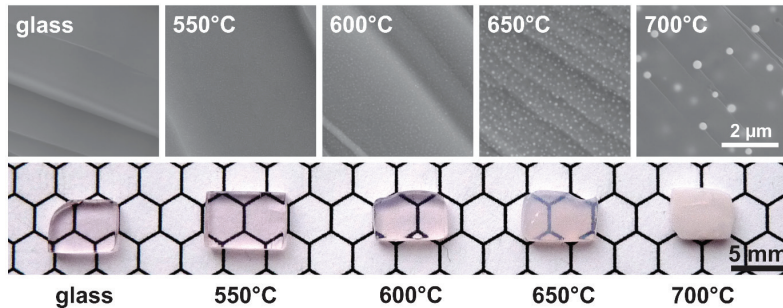The microstructure and photograph of precursor glass and glass ceramics containing $NaYF_4$: Er^{3+} are shown in Fig. 4.2.

Fig. 4.2. SEM micrographs (upper row) and photograph (lower row) of precursor glass and glass ceramics containing $NaYF_4$: Er^{3+} heat treated at 550–700 °C for 2 h.

No microheterogeneities were detected in the precursor glasses confirming the amorphous nature of precursors. The thermal treatment promoted the formation of spherical homogeneously distributed particles in the glass matrix. The lighter shade of particles indicates that they are enriched in heavier metal ions (RE^{3+} ions). TEM investigation of nanocrystalline glass ceramics revealed that the spherical particles are mostly single crystalline β-$NaREF_4$. The heat treatment at higher temperature favoured the growth of the particles, however the quantity of the crystallites diminished with the increase of temperature. This effect can be explained by reduced nucleation rate at higher temperature. The increase of the particle size after heat caused a gradual reduction of transparency due to the light scattering (See Fig. 4.2.). For optical applications larger crystallite size, which defines lower rate of non-radiative processes on the surface of the crystals, is preferable. Heat treatment at 600 °C for 1–2 h was found to be suitable for the preparation of transparent β-$NaREF_4$:Er^{3+} containing glass ceramics.

The phase formation in Na_2O-NaF-REF_3-Al_2O_3-SiO_2 based glass ceramics was found to be dependent on the type of rare earth ion and content in the precursor glass. Two solid solution systems $Na(La,Yb)F_4$:Er^{3+} and $Na(Gd,Lu)F_4$:Er^{3+} were investigated. In both systems, incorporation of high amount of lanthanides with smaller ionic radii (Yb, Lu) resulted in the formation of cubic α-$NaREF_4$ phases which can be associated with wider composition range of cubic phase and lower thermal stability of hexagonal phase in these systems. Unexpectedly cubic phase was efficiently stabilized even in lanthanum containing system, in which only hexagonal $NaLaF_4$ have been reported previously.

The X-ray diffraction data of $19Na_2O$-$3NaF$-$5LaF_3$-$6Al_2O_3$-$67SiO_2$: 1 mol% ErF_3, 0–3 mol% YbF_3 based glass ceramics with different Yb^{3+} content is shown in Fig. 4.3.

In precursor glasses containing LaF_3 hexagonal $NaLaF_4$ could be prepared, however, introduction of YbF_3 resulted in phase separation and formation of cubic phase with fluorite type structure. In similar lanthanum containing oxyfluoride systems isostructural fluorite type LaOF compounds have been detected previously, however, comparison of spectroscopic properties of all LaOF polymorphs and α-$NaYF_4$ with glass ceramics revealed that the fluorite type compound is indeed cubic Yb^{3+} stabilized $NaLaF_4$,which for now has only been prepared in oxyfluoride glass ceramics.
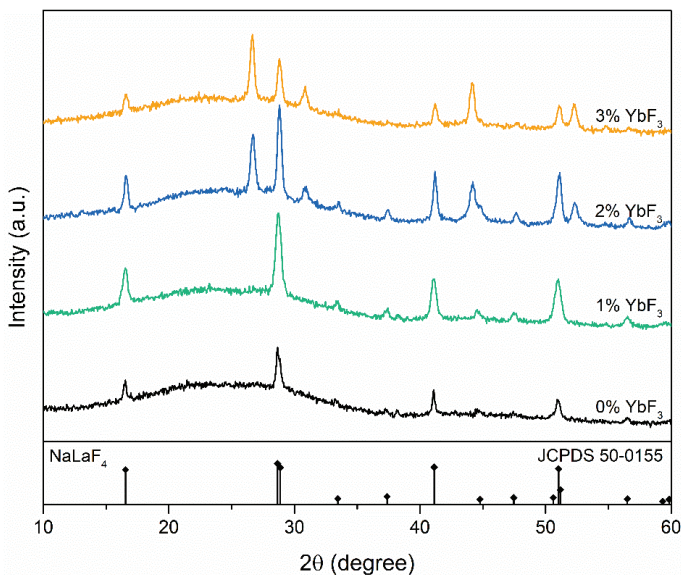

Fig. 4.3. X-ray diffraction patterns of glass ceramics containing 0–3% Yb^{3+} heat treated at 600 °C for 2 h

4.2. Luminescence spectroscopy of $NaREF_4$: Er^{3+} containing glass ceramics

In β-$NaREF_4$ containing glass ceramics intense UCL was detected. UCL spectra of precursor glass and glass ceramics containing β-$NaErF_4$ are shown in Fig. 4.4.

The UCL spectra of precursor glass consists of wide luminescence bands characteristic to Er^{3+} in amorphous environment. In glass ceramics narrow

luminescence bands characteristic to crystalline environment were detected confirming the incorporation of Er^{3+} in the fluoride nanocrystals. In addition to typical Er^{3+} UCL bands associated with two photon UCL ($^2H_{11/2} \rightarrow {}^4I_{15/2}$, $^4S_{3/2} \rightarrow {}^4I_{15/2}$ and $^4F_{9/2} \rightarrow {}^4I_{15/2}$) processes, luminescence bands characteristic to three photon UCL were detected in all $NaREF_4$ containing glass ceramics. The presence of three photon UCL bands in glass ceramics indicated considerable reduction of multiphonon relaxation rates in comparison to precursor glass. In addition, the UCL intensity of glass ceramics was up to two orders of magnitude higher than in the precursor glasses. Both of these effects are explained by an efficient incorporation of Er^{3+} ions in the low phonon environment of fluoride crystals, which reduce the non-radiative transition rate.
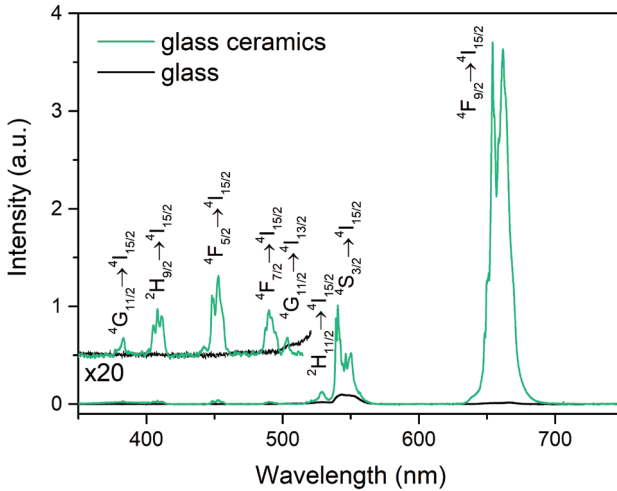

Fig. 4.4. UCL spectra of precursor glass and glass ceramics containing β-NaErF₄ excited at 975 nm.

UCL processes were investigated in all β-NaREF₄:Er^{3+} containing glass ceramics. Absorption spectrum of β-NaYF₄:Er^{3+} containing glass ceramics and partial energy level scheme of Er^{3+} ions with possible UCL mechanism are shown in Fig. 4.5.

In the investigated glass ceramics containing β-NaREF₄:Er^{3+} the dominant UCL mechanism was determined to be energy transfer between activator ions. In singly doped glass ceramics, Er^{3+} ions are promoted from ground state to $^4I_{11/2}$ emitting state by absorption of IR photons. Energy transfer between Er^{3+} ions ($^4I_{11/2};{}^4I_{11/2} \rightarrow {}^4I_{15/2};{}^4F_{7/2}$) results in the population of $^4F_{7/2}$ emitting level, from which rapid de-excitation populates $^2H_{11/2}$ and $^4S_{3/2}$ emitting states.

Large energy gap between $^4S_{3/2}$ and lower laying emitting states prevents efficient multiphonon relaxation in fluoride crystals, therefore $^2H_{11/2}$ and $^4S_{3/2}$ states are de-excited by radiative transitions and cross-relaxation. Due to relatively long lifetime of $^4S_{3/2}$ emitting state additional IR photon can promote Er^{3+} ions to higher energy levels resulting in the population of $^4G_{11/2}$, $^2H_{9/2}$, $^4F_{5/2}$ and $^4F_{7/2}$ emitting states, from which three photon UCL emission can be detected.
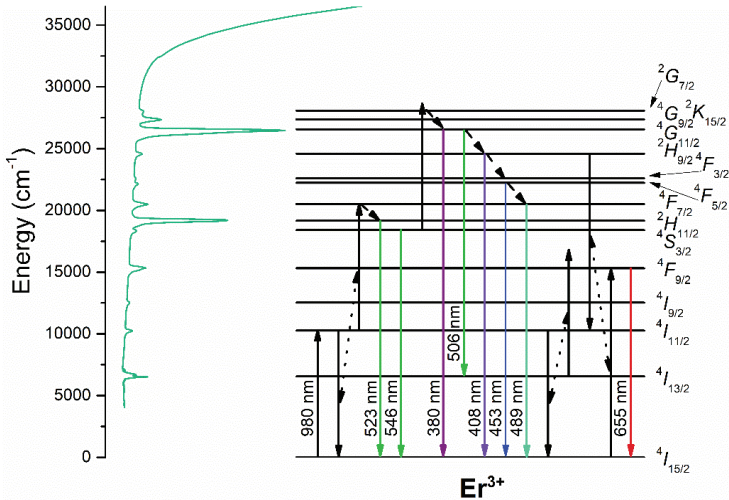

Fig. 4.5. Absorption spectrum of β-NaYF₄:Er³⁺ containing glass ceramics and partial energy level scheme of Er³⁺ ions

In the samples with high Er^{3+} content, such as β-NaErF₄ (shown in Fig. 4.4.), intense red UCL emission corresponding to $^4F_{9/2}{\rightarrow}^4I_{15/2}$ transition was detected. This emitting state is mainly populated by energy transfer and cross-relaxation processes. Using rate equation formalism in β-NaErF₄ two dominant processes ($^4I_{11/2}$;$^4I_{13/2}\rightarrow{}^4I_{15/2}$;$^4F_{9/2}$ and $^2H_{9/2}$;$^4I_{11/2}\rightarrow{}^4I_{11/2}$;$^4F_{9/2}$) were identified. Similar processes can be expected in all β-NaREF₄:Er³⁺ containing glass ceramics.

4.3. Site-selective spectroscopy of β-NaREF₄ containing glass ceramics

In Er^{3+} doped oxyfluoride glass ceramics two distinct decay processes were distinguished – rapid decay characteristic to Er^{3+} ions in glass matrix and slow decay characteristic to Er^{3+} ions in β-NaREF₄ crystals (see Fig. 4.6. a). The differences of luminescence decay in the glass and fluoride nanocrystals

were associated with deviations of phonon energy of both phases, which affect the multiphonon relaxation rates.

At low temperatures Er^{3+} ions in different crystalline environment can be selectively excited, therefore the spectroscopic properties of Er^{3+} in both glass and crystalline phase can be analyzed separately using site-selective spectroscopy. The luminescence spectra corresponding to Er^{3+} ions in glass (fast decay) and β-NaREF$_4$ nanocrystals (slow decay) are shown in Fig. 4.6. b.
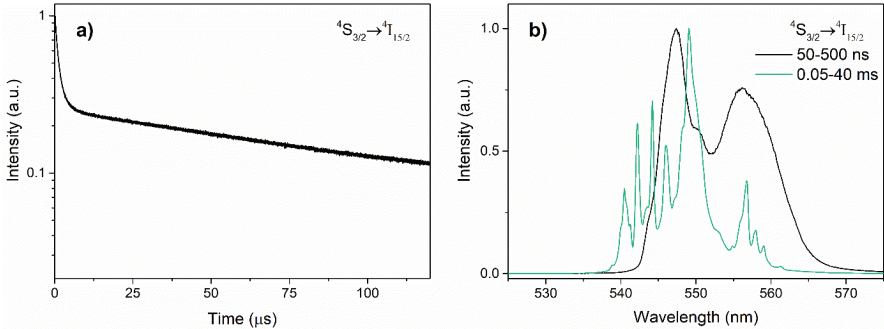

Fig. 4.6. a) Luminescence decay curve of the green emission ($^4S_{3/2} \rightarrow {}^4I_{15/2}$) and b) luminescence spectra corresponding to the fast (50–500 ns) and slow (0.05–40 ms) decay in β-NaErF$_4$ containing glass ceramics detected at 10 K.

In the crystalline environment, three distinct Er^{3+} luminescence spectra could be detected when the excitation wavelength was varied (see Fig. 4.7.).

These observations indicated that in β-NaREF$_4$ nanocrystals Er^{3+} is located in at least three distinct positions. Similar results have been obtained in polycrystalline β-NaREF$_4$ phases [113], [114]. In the crystalline structure of β-NaREF$_4$ there are only two distinct RE^{3+} positions, therefore two distinct luminescence spectra are expected in these phases (see Fig. 2.2.). The existence of the third position has been previously attributed to incorporation of activator ions in third cationic position half filled with Na$^+$ and vacancies [113], [114]. To test the validity of this assumption, the local environment of Er^{3+} was analyzed in β-NaErF$_4$ containing glass ceramics and polycrystalline single phase β-NaErF$_4$. Heterovalent substitution of Na$^+$ with RE^{3+} should not be efficient in β-NaREF$_4$ compounds containing high activator content, therefore the excitation efficiency of such position should be considerably lower in comparison to RE^{3+} positions characteristic to β-NaREF$_4$ lattice.

In β-NaErF$_4$ phases three distinct luminescence spectra with comparable excitation efficiency could be detected. The results suggest that the third Er^{3+} position detected in β-NaREF$_4$ compounds is not associated with incorporation of Er^{3+} ions Na$^+$ site. In β-NaREF$_4$ lattice there are two half-filled cationic

positions that create distortion in crystalline structure. We assume that this distortion modifies local environment of RE^{3+} sites causing the appearance of additional luminescence spectra. For further validation of this assumption, single crystals studies of β-NaREF$_4$ compounds are required, which are beyond the scope of this research.
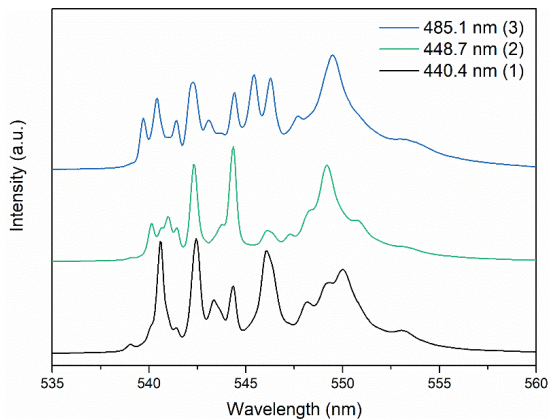

Fig. 4.7. Luminescence spectra of Er^{3+} ions in β-NaYF$_4$ containing glass ceramics detected at 10 K.

4.4. Crystallization of barium rare earth fluoride containing glasses

Introduction of BaF$_2$ in Na$_2$O-NaF-REF$_3$-Al$_2$O$_3$-SiO$_2$ glasses resulted in the formation of fluorite and fluorite-related phases. In this research the effect of BaF$_2$ and REF$_3$ ratio on the phase formation in YF$_3$ and YbF$_3$ containing glass ceramics were investigated in detail. XRD diffraction data of 15Na$_2$O-3NaF-(14-x)BaF$_2$-xYbF$_3$-6Al$_2$O$_3$-62SiO$_2$: 0.1% ErF$_3$ (x= 0-14 mol%) based glass ceramics heat treated at 650 °C for 2 h is shown in Fig. 4.8.

Two fluorite related phases – rhombohedrally distorted Ba$_4$RE$_3$F$_{17}$ and tetragonally distorted fluorite NaF-BaF$_2$-REF$_3$ compounds could be prepared in the investigated systems. This research was mainly focused on the investigation of Ba$_4$RE$_3$F$_{17}$ which was successfully prepared for RE=Gd, Y, Yb and Lu and was found to be suitable host for efficient UCL.

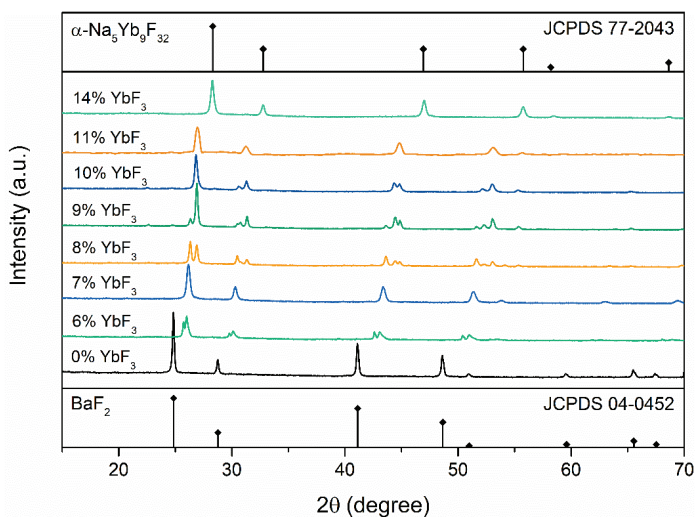**Fig. 4.8. XRD patterns of $15Na_2O\text{-}3NaF\text{-}(14\text{-}x)BaF_2\text{-}xYbF_3\text{-}6Al_2O_3\text{-}62SiO_2$: 0.1% ErF_3 (x= 0–14 mol%) based glass ceramics heat treated at 650 °C for 2 h.**

Typical thermal analysis curve of glass, in which $Ba_4RE_3F_{17}$ could be prepared is shown in Fig. 4.9. a)
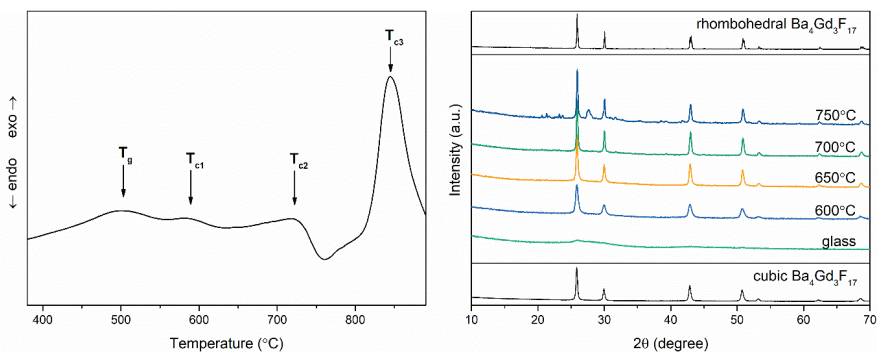
Fig. 4.9. a) DTA curve of precursor glass and b) XRD patterns of $Ba_4Gd_3F_{17}$ containing glass ceramics heat treated at 600–750 °C for 5 h.

In the precursor glass two exothermic effects associated with formation of fluoride crystalline phases (T_{c1} and T_{c2} in Fig. 4.9. a) could be detected. However, in XRD patterns (see Fig. 4.9. b) no changes in phase composition could be identified in this temperature range. It can be assumed that the second exothermic effect detected in DTA data could be associated with

order-disorder phase transition between the two modifications of $Ba_4RE_3F_{17}$. However, due to relatively small size of nanocrystals, the superstructure peaks associated with rhombohedral distortion rarely can be detected in nanocrystalline glass ceramics using XRD, therefore in the investigated glass ceramics site-selective spectroscopy was used to identify the phase transition (see section 4.8.).

4.5. Microstructure of Ba^{2+} containing glass ceramics

Most of Ba^{2+} containing glasses were relatively unstable and spontaneous crystallization occurred during the cooling of the melt. SEM micrographs of precursor glass and glass ceramics containing $Ba_4Gd_3F_{17}$: Er^{3+} are shown in Fig. 4.10.
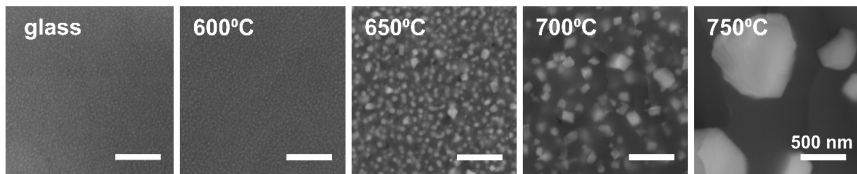

Fig. 4.10. SEM micrographs of precursor glass and glass ceramics containing $Ba_4Gd_3F_{17}$: Er^{3+} heat treated at 600–750 °C for 5 h.

Light grey particles enriched by heavy element ions (Ba^{2+} and RE^{3+}) could be observed in both precursor glass and glass ceramics, which is characteristic to spontaneous crystallization. The heat treatment of the glass resulted in a significant increase of particle size, however, the number of crystallites present in the material was significantly reduced. These results suggest Ostwald's ripening of nanoparticles during the heat treatment i.e. dissolution of smaller particles, ionic diffusion and re-deposition on larger particles.

The morphology of nanocrystals changed from spherical to rhombohedral with the increase of temperature of heat treatment, indirectly suggesting the formation of rhombohedral $Ba_4RE_3F_{17}$ at higher temperatures. In addition, unusually large crystals with size up to several hundreds of nm could be prepared in $Ba_4RE_3F_{17}$ containing glass ceramics. This effect could be associated to increase of Na^+ ions in oxide glass during the growth of fluoride nanocrystals, which significantly reduces the viscosity of glass matrix, therefore enabling efficient ionic diffusion required for rapid homogeneous crystallizations.

4.6. Upconversion luminescence in glass ceramics containing Ba$_4$RE$_3$F$_{17}$: Er^{3+}

Similar to β-NaREF$_4$, the formation of the crystalline phases in Ba^{2+} containing glass ceramics resulted in an enhancement of UCL emission. The highest UCL efficiency was determined for Ba$_4$RE$_3$F$_{17}$ phases which in Na$_2$O-BaF$_2$-YF$_3$-Al$_2$O$_3$-SiO$_2$:Er^{3+} system even surpassed β-NaREF$_4$. The higher emission efficiency could be attributed to suitable host matrix or optimal activator content in the crystalline phase. UCL spectra of Ba$_4$RE$_3$F$_{17}$: Er^{3+} (RE= Gd, Y, Yb, Lu) containing glass ceramics are shown in Fig. 4.11.

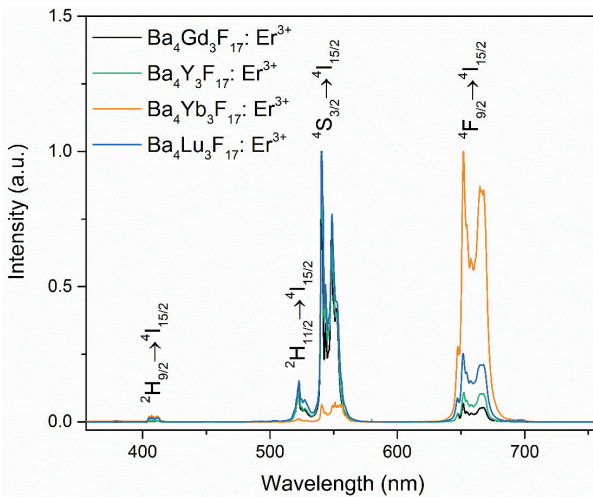**Fig. 4.11. UCL spectra of glass ceramics containing Ba$_4$RE$_3$F$_{17}$: Er^{3+} excited at 975 nm.**

The luminescence spectra of Ba$_4$RE$_3$F$_{17}$: Er^{3+} containing glass ceramics consist of typical luminescence bands of Er^{3+} characteristic to two and three photon UCL processes. The luminescence mechanism of Ba$_4$RE$_3$F$_{17}$: Er^{3+} (RE= Gd, Y Lu) is assumed to be similar to β-NaREF$_4$ compounds (see section 4.2.). The deviations in red and green emission ratio of these glass ceramics could be ascribed to changes of Er^{3+} content in the crystalline phase.

In the case of Ba$_4$Yb$_3$F$_{17}$: Er^{3+}, unusually intense red UCL was detected. This effect was investigated in details.

The UCL intensity I is proportional to n-th power of pump power P, where n is the number of photons required to populate the emitting states. This statement is valid in case of small energy transfer rates and the value of n is less than the number of required photons in most systems [115]. The power dependence of UCL intensity of red and green emission in the glass ceramics containing Ba$_4$Yb$_3$F$_{17}$: Er^{3+} are shown in Fig. 4.12.
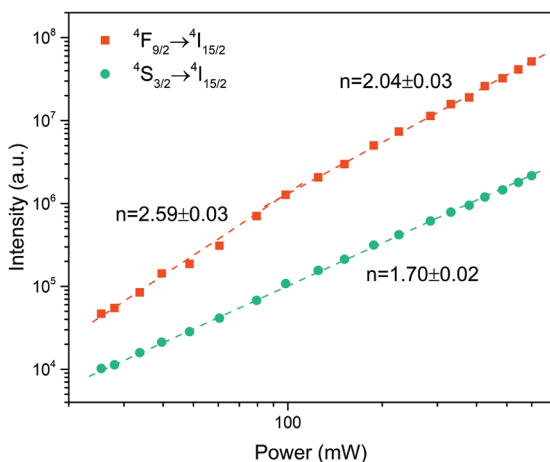
Fig. 4.12. Power dependence of UCL intensity of red and green emission in the glass ceramics containing $Ba_4Yb_3F_{17}$: Er^{3+}. UCL is excited with 975 nm.

The slope of log-log power dependence for the green emission $n=1.7\pm0.02$ is close to 2.0 which it is characteristic to two photon UCL process. However, value of the red emission $n=2.59\pm0.03$ for low power region suggests that three photon UCL process is involved in the population of this emitting state. To determine the dominant UCL mechanism, PL excitation and luminescence kinetics were analysed.
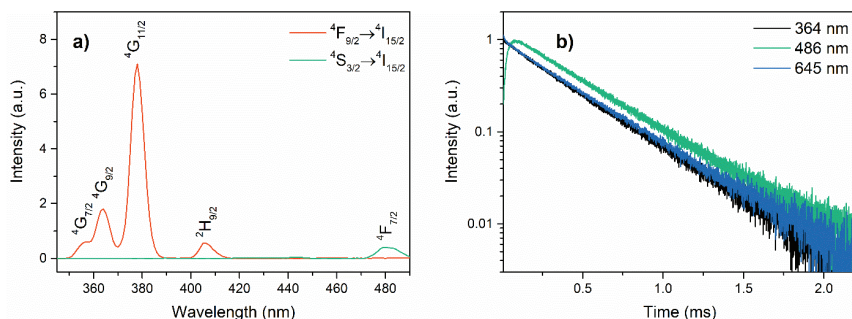
Fig. 4.13. a) Luminescence excitation spectra for $^4S_{3/2}{\rightarrow}^4I_{15/2}$ (green) and $^4F_{9/2}{\rightarrow}^4I_{15/2}$ (red) emission and b) luminescence kinetics of $^4F_{9/2}{\rightarrow}^4I_{15/2}$ (red) emission excited at 364, 486 and 645 nm of $Ba_4Yb_3F_{17}$: Er^{3+} containing glass ceramics.

The analysis of PL excitation spectra revealed that the green emission can be detected after the excitation of $^4I_{15/2}{\rightarrow}^4F_{7/2}$ band but the red emission can be unusually efficiently excited in region from 350 to 420 nm (see Fig. 4.13. a). The results suggest that the excited states in ultraviolet spectral range are

31

involved in three photon UCL process resulting in efficient red UCL emission ($^4F_{9/2} \rightarrow {}^4I_{15/2}$) and indicate that processes bypassing $^4F_{7/2}$ excited state such as cross-relaxation is involved in the population of red emitting state ($^4F_{9/2}$). To confirm this assumption, luminescence kinetics of $^4F_{9/2} \rightarrow {}^4I_{15/2}$ transition were analysed.

Non-exponential luminescence kinetics with a rise of luminescence intensity after laser impulse was detected for the red emission ($^4F_{9/2} \rightarrow {}^4I_{15/2}$) when $^4F_{7/2}$ emitting state was excited (486 nm excitation) indicating that the energy transfer is involved in the population of $^4F_{9/2}$ emitting state (see Fig. 4.13. b). Possible cross-relaxation and energy transfer mechanisms are shown in Fig. 4.5.

Identic rapid exponential luminescence kinetics were detected for the red emission after excitation $^4G_{7/2}$, $^4G_{9/2}$, $^4G_{11/2}$ and $^2H_{9/2}$ states. As an example luminescence kinetics of red emission after excitation of $^4G_{9/2}$ emitting state (364 nm excitation) are shown in Fig. 4.13. b. They were found to be identic to the lifetime of $^4F_{9/2}$ emitting state (645 nm excitation). Two non-radiative processes could be involved in the population of $^4F_{9/2}$ emitting state – multiphonon relaxation and cross-relaxation. The multiphonon relaxation is step by step process that would not result in the bypass of $^4F_{7/2}$ excited state, therefore the results confirm that $^4F_{9/2}$ is populated by cross-relaxation process. Due to high Yb^{3+} content in the crystalline phase, cross-relaxation between Er^{3+} and Yb^{3+} can be expected. $^2H_{9/2} \rightarrow {}^4F_{9/2}$ transition of Er^{3+} is resonant with $^2F_{7/2} \rightarrow {}^2F_{5/2}$ transition of Yb^{3+}, therefore rapid cross-relaxation ($^2H_{9/2}, {}^4F_{7/2} \rightarrow {}^4F_{9/2}, {}^4F_{5/2}$) can occur.

The dominant UCL mechanism of $Ba_4Yb_3F_{17}$:Er^{3+} is summarized in Fig. 4.14.

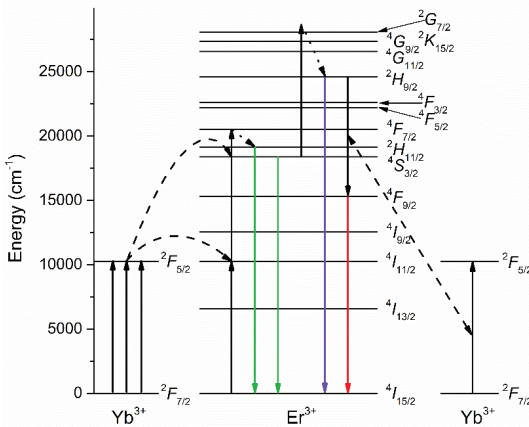**Fig. 4.14. Partial energy level scheme and dominant UCL mechanisms in Ba₄Yb₃F₁₇: Er³⁺ containing glass ceramics**

The infrared excitation promotes Yb^{3+} to its excited state ($^2F_{7/2} \rightarrow ^2F_{5/2}$). This transition is resonant with $^4I_{15/2} \rightarrow ^4I_{11/2}$ and $^4I_{11/2} \rightarrow ^4F_{7/2}$ transitions of Er^{3+}. Energy transfer from Yb^{3+} to Er^{3+} results in population of $^4F_{7/2}$, which rapidly de-excites to $^2H_{11/2}$ and $^4S_{3/2}$ emitting states, from which green emission is detected. This emission is predominantly two photon process as suggested by power dependence data shown in Fig. 4.12. Due to relatively long lifetime of green emitting states, Er^{3+} ions can be further exited to $^2G_{7/2}$ by absorption of third infrared photon. Rapid multiphonon relaxation for $^4G_{7/2}$, $^4G_{9/2}$ and $^4G_{11/2}$ to $^2H_{9/2}$ is expected in the fluoride hosts. From this excited state efficient cross-relaxation with Yb^{3+} occurs ($^2H_{9/2}, ^4F_{7/2} \rightarrow ^4F_{9/2}, ^4F_{5/2}$), which populate the red emitting state $^4F_{9/2}$ and results in intense red three photon UCL emission.

4.7. Incorporation efficiency of rare earth ions in $Ba_4RE_3F_{17}$ containing glass ceramics

In $Ba_4Lu_3F_{17}$ containing glass ceramics considerable changes in the UCL band relative intensity was observed when the Er^{3+} content was varied. Photograph of transparent $Ba_4Lu_3F_{17}$:Er^{3+} containing glass ceramics in ambient light and samples excited with 975 nm are shown in Fig. 4.15.
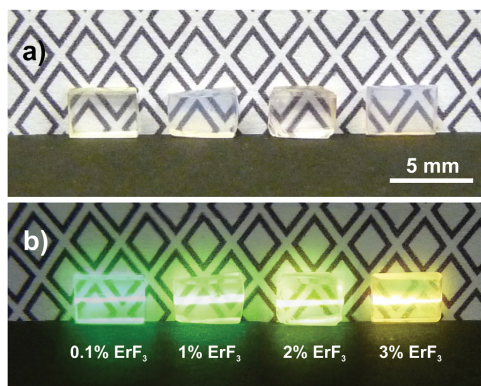
Fig. 4.15. a) Photograph of glass ceramics containing $Ba_4Lu_3F_{17}$:Er^{3+} in a) ambient light and b) excited with 975 nm.

The increase of red emission in glass ceramics containing higher activator content is attributed to enhancement of energy transfer processes that increase the population of the red emitting state (see Fig. 4.5. β-NaREF₄). The efficiency of such processes mainly depends on the Er^{3+} content in the materials, therefore this effect was used in glass ceramics to quantitatively determine Er^{3+} content in $Ba_4Lu_3F_{17}$: Er^{3+} nanocrystals. The luminescence band relative intensity ratio and luminescence kinetics of glass ceramics were

compared to microcrystalline $Ba_4Lu_3F_{17}$:Er^{3+} prepared using hydrothermal synthesis and heat treatment. This process is described in details elsewhere [116]. The deviations in effective decay time of green emission and relative intensity ratio of green and red emission of microcrystalline $Ba_4Lu_3F_{17}$:Er^{3+} excited with 445 nm is shown in Fig. 4.16.
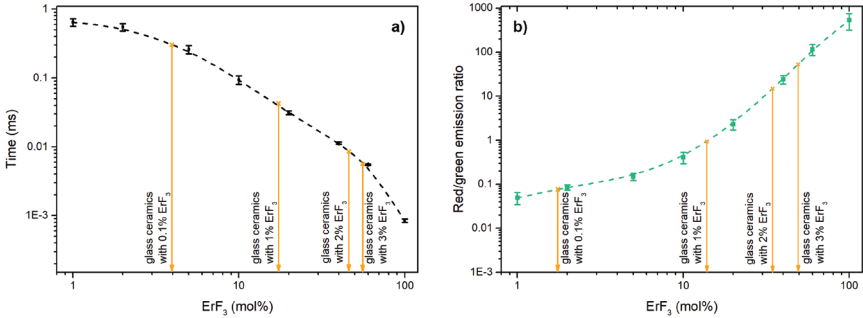
Fig. 4.16. a) the effective decay time of green emission and b) red/green emission ratio of microcrystalline $Ba_4Lu_3F_{17}$:Er^{3+} excited with 445 nm. Droplines indicate values detected in $Ba_4Lu_3F_{17}$:Er^3 containing glass ceramics.

In oxyfluoride glass ceramics RE^{3+} ions are predominantly incorporated in fluoride-rich phase [1], therefore during the crystallization of $Ba_4Lu_3F_{17}$:Er^{3+} in glass ceramics, the Lu^{3+}/ Er^{3+} ratio is expected to be similar to that present in the precursor glass. The expected Er^{3+} content, which is based on chemical composition of the precursor glass and values estimated from comparison of spectroscopic properties of glass ceramics with microcrystalline samples are shown in Table 4.1.

Table 4.1.

Expected and estimated Er^{3+} content in $Ba_4Lu_3F_{17}$: Er^{3+} nanocrystals formed in oxyfluoride glasses

ErF_3 in precursor glass (mol%)	Er^{3+} content in $Ba_4Lu_3F_{17}$ nanocrystals (mol%)	
	Expected	Estimated
0.1	1.4	2.8±1.1
1	14.3	15.8±2.1
2	28.6	39.4±5.2
3	42.9	52.2±2.8

The estimated Er^{3+} content in $Ba_4Lu_3F_{17}$ nanocrystals exceeded the expected values. These results indicate preferential incorporation of Er^{3+} over Lu^{3+} in fluoride crystals. Acording to the studies of partitioning coeficients of RE^{3+} ions in imisscible fluoride and silicate melts, incorporation efficiency of

RE^{3+} ions in fluoride melts slightly increases from Lu^{3+} to La^{3+} [78], [117]. To test this effect in oxyfluoride glasses, Er^{3+} distribution in glass ceramics containing Ba$_4$Gd$_3$F$_{17}$: Er^{3+}, Ba$_4$Y$_3$F$_{17}$:Er^{3+} and Ba$_4$Lu$_3$F$_{17}$:Er^{3+} were compared using site-selective spectroscopy. The excitation spectra for the fast and slow components of the green luminescence (corresponding to Er^{3+} in the glass and crystalline phase) in the glass ceramics systems containing different Ba$_4$RE$_3$F$_{17}$ nanocrystals are shown in Fig. 4.17.
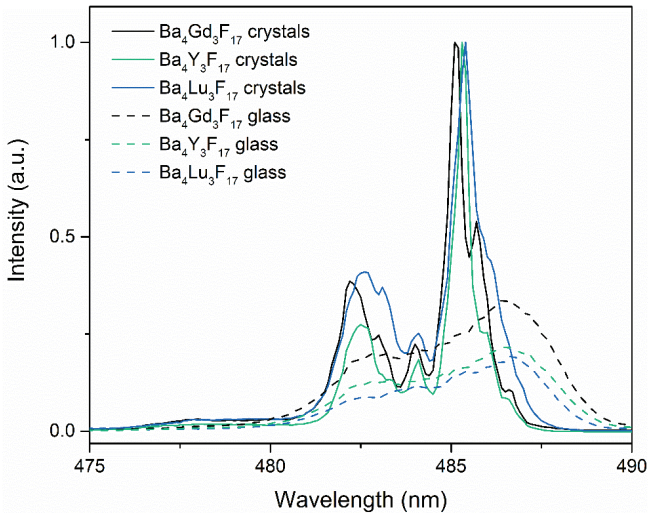
Fig. 4.17. Time-resolved luminescence excitation spectra of Er^{3+} ion ^{4}S$_{3/2}$ emission in glass and Ba$_4$RE$_3$F$_{17}$ nanocrystals formed in oxyfluoride glass ceramics doped with 1% Er^{3+} detected at 10 K.

In all three investigated glass ceramics, the relative efficiency of excitation bands in both glass and crystalline phase was calculated and compared between the Ba$_4$RE$_3$F$_{17}$ containing glass ceramics. The lowest excitation efficiency in glass phase was found in Ba$_4$Lu$_3$F$_{17}$ containing glass ceramics and it was approximately 14% lower than Ba$_4$Y$_3$F$_{17}$ and 36% lower than Ba$_4$Gd$_3$F$_{17}$.

The luminescence data agree well with experimental observations in phase separated oxyfluoride melts [117] and confirm the assumption of preferential incorporation of RE^{3+} ions in fluoride phase following the trend Lu^{3+}< La^{3+}. The results suggest that in the glass ceramics containing multiple RE^{3+} ions, activator with larger ionic radius than RE^{3+} in host matrix is required to ensure efficient incorporation activator in crystalline phase.

4.8. Site selective spectroscopy of Er³⁺ in Ba₄RE₃F₁₇ containing glass ceramics

In Ba₄RE₃F₁₇ containing glass ceramics structural changes in the fluoride phase were expected during the crystallization of the glass but could not be confirmed using X-ray diffraction data (see section 4.4.). In order to investigate this effect, local environment of Er³⁺ in glass ceramics containing Ba₄RE₃F₁₇: Er³⁺ was analysed. The site-selective luminescence spectra of glass ceramics containing Ba₄Gd₃F₁₇: Er³⁺ and Ba₄Lu₃F₁₇:Er³⁺ heat treated at 550 °C and 700 °C are shown in Fig. 4.18.
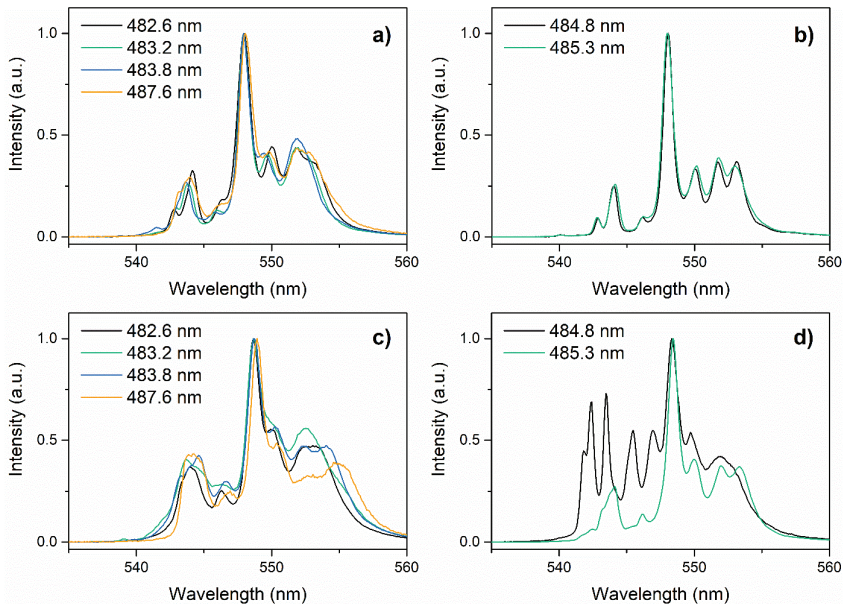
Fig. 4.18. Luminescence spectra of Er³⁺ ions in glass ceramic containing a–b) Ba₄Gd₃F₁₇ heat treated at 550 °C and b) 700 °C for 5 h and c–d) Ba₄Lu₃F₁₇ heat treated at c) 550 °C and d) 700 °C for 2 h detected at 10 K.

The luminescence spectra of Er³⁺ in the crystalline environment of the glass ceramics heat treated at lower temperature (see Fig. 4.18. a and c) consisted of many similar but distinct luminescence spectra suggesting the incorporation of Er³⁺ in distorted environment characteristic to metastable cubic Ba₄RE₃F₁₇ (see section 2.3.). After the heat treatment at higher temperature one (in the case of Ba₄Gd₃F₁₇ and Ba₄Y₃F₁₇) or two (in the case of Ba₄Yb₃F₁₇ and Ba₄Lu₃F₁₇) distinct luminescence spectra could be observed indicating the ordering of the local structure (see Fig. 4.18. b and d).

In rhombohedral $Ba_4RE_3F_{17}$ all RE^{3+} positions are equivalent [118], therefore, in Er^{3+} doped $Ba_4RE_3F_{17}$ single Er^{3+} position is expected, which agree well with the experimental data of $Ba_4Gd_3F_{17}$:Er^{3+} and $Ba_4Y_3F_{17}$:Er^{3+} containing glass ceramics. However, in $Ba_4Yb_3F_{17}$ and $Ba_4Lu_3F_{17}$ containing glass ceramics and microcrystalline single-phase materials, two distinct Er^{3+} positions were detected. The crystal structure of $Ba_4RE_3F_{17}$ consists of $Ba_8[RE_6F_{68-69}]$ superclusters (see section 2.3.), which are the most common superclusters in BaF_2-REF_3 solid solutions [42]. Recently in single crystal studies of cubic BaF_2-REF_3 (RE=Yb, Lu) compounds new type of supercluster $RE_8[Ba_6F_{71}]$ (octahedral alkali earth supercluster) was determined [119]. We assume that such clusters could be present in the cubic and rhombohedral $Ba_4RE_3F_{17}$ (RE=Yb, Lu), however, for the confirmation of this assumption single crystal studies of these phases are required.

The deviations in Er^{3+} luminescence spectra of the glass ceramics heat treated at different temperatures confirmed order-disorder phase transitions in $Ba_4RE_3F_{17}$ containing glass ceramics and were used to determine phase transition temperature. Luminescence spectra of the precursor glass and glass ceramics containing $Ba_4Gd_3F_{17}$: Er^{3+} and $Ba_4Lu_3F_{17}$: Er^{3+} heat treated at various temperatures are shown in Fig. 4.19.
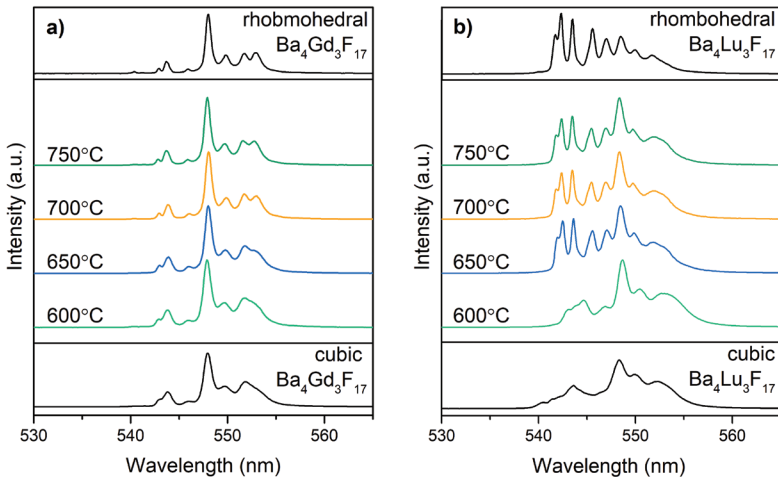
Fig. 4.19. Luminescence spectra of glass ceramics containing a) $Ba_4Gd_3F_{17}$: Er^{3+} and b) $Ba_4Lu_3F_{17}$: Er^{3+} detected at 10 K.

Changes associated with ordering of $Ba_4RE_3F_{17}$ structure could be easily detected in the glass ceramics using Er^{3+} as a probe. The results suggest that the order-disorder phase transition slightly deviated for $Ba_4RE_3F_{17}$ compounds and ranged from 600–700 °C.

CONCLUSIONS

1. Na_2O-NaF-REF_3-Al_2O_3-SiO_2 and Na_2O-NaF-BaF_2-REF_3-Al_2O_3-SiO_2 based glasses were found to be suitable precursors for the preparation of transparent glass ceramics containing $NaREF_4$ and $Ba_4RE_3F_{17}$ nanocrystals.
2. In glass ceramics containing $NaREF_4$ nanocrystals two polymorphic modifications (α-$NaREF_4$ and β-$NaREF_4$) could be prepared. The phase composition could be controlled by selecting suitable heat treatment or by changing the chemical composition of precursor glass.
3. In $Ba_4RE_3F_{17}$ containing glass ceramics order-disorder phase transition from metastable cubic to rhombohedrally distorted cubic $Ba_4RE_3F_{17}$ was identified using site-selective spectroscopy. The phase transition was identified in temperature range 600–700 °C.
4. Er^{3+} was proven to be suitable probe for the analysis of crystallization processes, local environment and activator distribution in the glass ceramics. The comparison of luminescence relative intensity ratio and luminescence kinetics of glass ceramics with microcrystalline single phase compounds was successfully used to quantitatively determine Er^{3+} content in $Ba_4Lu_3F_{17}$: Er^{3+} nanocrystals formed in glass ceramics.
5. In the investigated glass ceramics, efficient UCL emission could be achieved resulting from energy transfer between Er^{3+} ions in fluoride nanocrystals. The highest emission intensity was achieved in $Ba_4Lu_3F_{17}$:Er^{3+} containing glass ceramics, which combine low phonon energy, low local symmetry and efficient incorporation of Er^{3+} in the crystalline phase. Unusually intense red UCL was detected in $Ba_4Yb_3F_{17}$: Er^{3+} containing glass ceramics resulting from three photon UCL process.

THESES

- In the glass ceramics containing $NaLaF_4$: Er^{3+}, Yb^{3+} increase of Yb^{3+} content promotes the formation of cubic fluorite type $NaLaF_4$, which currently has been obtained only in oxyfluoride glass ceramics.
- In the crystalline environment of β-$NaREF_4$: Er^{3+} (RE=rare earth ion) containing glass ceramics two Er^{3+} positions are associated with incorporation of erbium ions in the rare earth ion positions and the third is related to distortion of these sites caused by half-filled cationic positions.
- In $Ba_4RE_3F_{17}$: Er^{3+} containing glass ceramics variations in the local environment of Er^{3+} ions are associated with the phase transition from metastable cubic to rhombohedrally-distorted cubic $Ba_4RE_3F_{17}$.
- In $Ba_4Yb_3F_{17}$: Er^{3+} containing glass ceramics unusually intense red upconversion luminescence is attributed to three photon energy transfer from Yb^{3+} to Er^{3+}, followed by multiphonon relaxation and cross-relaxation between Er^{3+} and Yb^{3+}.
- In oxyfluoride glass ceramics the Er^{3+} content in the crystalline phase can be determined by comparing luminescence band intensity ratio and luminescence kinetics of Er^{3+} in glass ceramics and microcrystalline fluoride crystals with known activator content.

REFERENCES

[1]   P. P. Fedorov, A. A. Luginina, and A. I. Popov, "Transparent oxyfluoride glass ceramics," *J. Fluor. Chem.*, vol. 172, pp. 22–50, Apr. 2015, doi: 10.1016/j.jfluchem.2015.01.009.

[2]   J. Qiu, Q. Jiao, D. Zhou, and Z. Yang, "Recent progress on upconversion luminescence enhancement in rare-earth doped transparent glass-ceramics," *J. Rare Earths*, vol. 34, no. 4, pp. 341–367, Apr. 2016, doi: 10.1016/S1002-0721(16)60034-0.

[3]   G. Liu, "Advances in the theoretical understanding of photon upconversion in rare-earth activated nanophosphors," *Chem. Soc. Rev.*, vol. 44, no. 6, pp. 1635–1652, 2015, doi: 10.1039/C4CS00187G.

[4]   A. de Pablos-Martín *et al.*, "Design of oxy-fluoride glass-ceramics containing NaLaF$_4$ nano-crystals," *J. Non. Cryst. Solids*, vol. 356, no. 52–54, pp. 3071–3079, Dec. 2010, doi: 10.1016/j.jnoncrysol.2010.04.057.

[5]   F. Xin *et al.*, "Up-conversion luminescence of Er^{3+}-doped glass ceramics containing β-NaGdF$_4$ nanocrystals for silicon solar cells," *Mater. Lett.*, vol. 78, pp. 75–77, Jul. 2012, doi: 10.1016/j.matlet.2012.03.037.

[6]   F. Auzel, "Upconversion and Anti-Stokes Processes with f and d Ions in Solids," *Chem. Rev.*, vol. 104, no. 1, pp. 139–174, Jan. 2004, doi: 10.1021/cr020357g.

[7]   H. Scheife, G. Huber, E. Heumann, S. Bär, and E. Osiac, "Advances in up-conversion lasers based on Er^{3+} and Pr^{3+}," *Opt. Mater. (Amst).*, vol. 26, no. 4, pp. 365–374, Sep. 2004, doi: 10.1016/j.optmat.2003.10.010.

[8]   H. Zhu, X. Chen, L. M. Jin, Q. J. Wang, F. Wang, and S. F. Yu, "Amplified Spontaneous Emission and Lasing from Lanthanide-Doped Up-Conversion Nanocrystals," *ACS Nano*, vol. 7, no. 12, pp. 11420–11426, Dec. 2013, doi: 10.1021/nn405387t.

[9]   E. Downing, L. Hesselink, J. Ralston, and R. Macfarlane, "A Three-Color, Solid-State, Three-Dimensional Display," *Science (80-.).*, vol. 273, no. 5279, pp. 1185–1189, Aug. 1996, doi: 10.1126/science.273.5279.1185.

[10] H. H. Refai, "Static Volumetric Three-Dimensional Display," *J. Disp. Technol.*, vol. 5, no. 10, pp. 391–397, Oct. 2009, doi: 10.1109/JDT.2009.2027911.

[11] Y. Zhou, S.-T. Han, X. Chen, F. Wang, Y.-B. Tang, and V. A. L. Roy, "An upconverted photonic nonvolatile memory," *Nat. Commun.*, vol. 5, no. 1, p. 4720, Dec. 2014, doi: 10.1038/ncomms5720.

[12] W. Xu, H. Zhao, Z. Zhang, and W. Cao, "Highly sensitive optical thermometry through thermally enhanced near infrared emissions from Nd^{3+}/Yb^{3+} codoped oxyfluoride glass ceramic," *Sensors Actuators B Chem.*, vol. 178, pp. 520–524, Mar. 2013, doi: 10.1016/j.snb.2012.12.050.

[13] J.-C. Boyer, C.-J. Carling, B. D. Gates, and N. R. Branda, "Two-Way Photoswitching Using One Type of Near-Infrared Light, Upconverting Nanoparticles, and Changing Only the Light Intensity," *J. Am. Chem. Soc.*, vol. 132, no. 44, pp. 15766–15772, Nov. 2010, doi: 10.1021/ja107184z.

[14] A. Shalav, B. S. Richards, and M. A. Green, "Luminescent layers for enhanced silicon solar cell performance: Up-conversion," *Sol. Energy Mater. Sol. Cells*, vol. 91, no. February, pp. 829–842, 2007, doi: 10.1016/j.solmat.2007.02.007.

[15] D. Chen, Z. Wan, and Y. Zhou, "Dual-phase nano-glass-ceramics for optical thermometry," *Sensors Actuators, B Chem.*, vol. 226, pp. 14–23, 2016, doi: 10.1016/j.snb.2015.10.115.

[16] K. Presley *et al.*, "Nanoscale upconversion for oxygen sensing," *Mater. Sci. Eng. C*, vol. 70, pp. 76–84, Jan. 2017, doi: 10.1016/j.msec.2016.08.056.

[17] W. Wu, L. Yao, T. Yang, R. Yin, F. Li, and Y. Yu, "NIR-light-induced deformation of cross-linked liquid-crystal polymers using upconversion nanophosphors," *J. Am. Chem. Soc.*, vol. 133, no. 40, pp. 15810–15813, 2011, doi: 10.1021/ja2043276.

[18] Z. Gu, L. Yan, G. Tian, S. Li, Z. Chai, and Y. Zhao, "Recent Advances in Design and Fabrication of Upconversion Nanoparticles and Their Safe Theranostic Applications," *Adv. Mater.*, vol. 25, no. 28, pp. 3758–3779, Jul. 2013, doi: 10.1002/adma.201301197.

[19] N. M. Idris, M. K. Gnanasammandhan, J. Zhang, P. C. Ho, R. Mahendran, and Y. Zhang, "In vivo photodynamic therapy using upconversion nanoparticles as remote-controlled nanotransducers.," *Nat. Med.*, vol. 18, no. 10, pp. 1580–5, Oct. 2012, doi: 10.1038/nm.2933.

[20] M. Wang, G. Abbineni, A. Clevenger, C. Mao, and S. Xu, "Upconversion nanoparticles: synthesis, surface modification and biological applications," *Nanomedicine Nanotechnology, Biol. Med.*, vol. 7, no. 6, pp. 710–729, Dec. 2011, doi: 10.1016/j.nano.2011.02.013.

[21] C. R. Ronda, *Luminescence*. Weinheim, Germany: Wiley-VCH Verlag GmbH & Co. KGaA, 2007.

[22] M.-F. Joubert, S. Guy, B. Jacquier, and C. Linarés, "The photon-avalanche effect: review, model and application," *Opt. Mater. (Amst).*, vol. 4, no. 1, pp. 43–49, Dec. 1994, doi: 10.1016/0925-3467(94)90054-X.

[23] J. C. Goldschmidt and S. Fischer, "Upconversion for Photovoltaics – a Review of Materials, Devices and Concepts for Performance Enhancement," *Adv. Opt. Mater.*, vol. 3, no. 4, pp. 510–535, Apr. 2015, doi: 10.1002/adom.201500024.

[24] F. Wang and X. Liu, "Recent advances in the chemistry of lanthanide-doped upconversion nanocrystals," *Chem. Soc. Rev.*, vol. 38, no. 4, p. 976, Apr. 2009, doi: 10.1039/b809132n.

[25] B. P. Sobolev, "Non-stoichiometry in inorganic fluorides and phases with fluorite structure," *Butll. Soc. Cat. Cien.*, vol. 12, no. 2, pp. 275–332, May 1991.

[26] K. W. Kra *et al.*, "Hexagonal Sodium Yttrium Fluoride Based Green and Blue Emitting Upconversion Phosphors," *Chem. Mater.*, vol. 16, no. 5, pp. 1244–1251, 2004, doi: 10.1021/cm031124o.

[27] P. P. Fedorov, "Systems of Alkali and Rare-Earth Metal Fluorides," *Russ. J. Inorg. Chem.*, vol. 44, no. April, pp. 1703–1727, 1999.

[28] D. M. Roy and R. Roy, "Controlled Massively Defective Crystalline Solutions with the Fluorite Structure," *J. Electrochem. Soc.*, vol. 111, p. 421, 1964, doi: 10.1149/1.2426145.

[29] A. Grzechnik, P. Bouvier, M. Mezouar, M. D. Mathews, A. K. Tyagi, and J. Köhler, "Hexagonal $Na_{1.5}Y_{1.5}F_6$ at High Pressures," *J. Solid State Chem.*, vol. 165, no. 1, pp. 159–164, Apr. 2002, doi: 10.1006/jssc.2001.9525.

[30] D. Tu, Y. Liu, H. Zhu, R. Li, L. Liu, and X. Chen, "Breakdown of crystallographic site symmetry in lanthanide-doped $NaYF_4$ crystals," *Angew. Chemie – Int. Ed.*, vol. 52, no. 4, pp. 1128–1133, 2013, doi: 10.1002/anie.201208218.

[31] C. Renero-Lecuna *et al.*, "Origin of the High Upconversion Green Luminescence Efficiency in β-$NaYF_4$:2%Er^{3+} , 20%Yb^{3+}," *Chem. Mater.*, vol. 23, no. 15, pp. 3442–3448, Aug. 2011, doi: 10.1021/cm2004227.

[32] Jiazhong Zhang, Haiping Xia, Yongzhang Jiang, Shuo Yang, Haochuan Jiang, and Baojiu Chen, "Efficient Quantum Cutting in Tb^{3+} /Yb^{3+} Codoped α-$NaYF_4$ Single Crystals Grown by Bridgman Method Using KF Flux for Solar Photovoltaic," *IEEE J. Quantum Electron.*, vol. 51, no. 6, pp. 1–6, Jun. 2015, doi: 10.1109/ JQE.2015.2418756.

[33] M. M. Lage, F. M. Matinaga, J. Gesland, and R. L. Moreira, "Optical phonon modes and crystal structure of $NaLaF_4$ single crystals Optical phonon modes and crystal structure of $NaLaF_4$ single crystals," vol. 053510, 2006, doi: 10.1063/1.2177380.

[34] J. L. Sommerdijk, "Influence of host lattice on the infrared-excited visible luminescence in Yb^{3+}, Er^{3+}-doped fluorides," *J. Lumin.*, vol. 6, no. 1, pp. 61–67, Jan. 1973, doi: 10.1016/0022-2313(73)90095-1.

[35] L. Wang *et al.*, "A New Cubic Phase for a $NaYF_4$ Host Matrix Offering High Upconversion Luminescence Efficiency," *Adv. Mater.*, vol. 27, no. 37, pp. 5528–5533, 2015, doi: 10.1002/adma.201502748.

[36] M. M. Lage, R. L. Moreira, F. M. Matinaga, and J.-Y. Gesland, "Raman and Infrared Reflectivity Determination of Phonon Modes and Crystal Structure of Czochralski-Grown $NaLnF_4$ (Ln = La, Ce, Pr, Sm, Eu, and Gd) Single Crystals," *Chem. Mater.*, vol. 17, no. 17, pp. 4523–4529, Aug. 2005, doi: 10.1021/cm050860k.

[37] M. P. Miller and J. C. Wright, "Single site multiphonon and energy transfer relaxation phenomena in BaF_2:Er^{3+}," *J. Chem. Phys.*, vol. 68, no. 4, pp. 1548–1562, Feb. 1978, doi: 10.1063/1.435924.

[38] M. Schlesinger and G. W. F. Drake, "On the vibronic spectrum of rare earths in calcium fluoride," *Can. J. Phys.*, vol. 54, no. 16, pp. 1699–1701, Aug. 1976, doi: 10.1139/p76-202.

[39] D. N. Patel, R. B. Reddy, and S. K. Nash-Stevenson, "Diode-pumped violet energy upconversion in BaF_2:Er^{3+}," *Appl. Opt.*, vol. 37, no. 33, p. 7805, Nov. 1998, doi: 10.1364/AO.37.007805.

[40] G. Krieke, A. Sarakovskis, R. Ignatans, and J. Gabrusenoks, "Phase transitions and upconversion luminescence in oxyfluoride glass ceramics containing $Ba_4Gd_3F_{17}$ nanocrystals," *J. Eur. Ceram. Soc.*, vol. 37, no. 4, pp. 1713–1722, Apr. 2017, doi: 10.1016/j.jeurceramsoc.2016.12.023.

[41] S. V Kuznetsov, P. P. Fedorov, V. V Voronov, K. S. Samarina, R. P. Ermakov, and V. V Osiko, "Synthesis of $Ba_4R_3F_{17}$ (R stands for rare-earth elements) powders and transparent compacts on their base," *Russ. J. Inorg. Chem.*, vol. 55, no. 4, pp. 484–493, Apr. 2010, doi: 10.1134/S0036023610040029.

[42] P. P. Fedorov, "Association of point defects in non-stoichiometric $M_{1-x}R_xF_{2+x}$ fluorite-type solid solutions," *Butll. Soc. Cat. Cien.*, vol. XII, no. 2, pp. 349–381, 1991.

[43] J. Grube and G. Krieke, "How activator ion concentration affects spectroscopic properties on $Ba_4Y_3F_{17}$: Er^{3+}, Yb^{3+}, a new perspective up-conversion material," *J. Lumin.*, vol. 203, no. October 2017, pp. 376–384, 2018, doi: 10.1016/j.jlumin.2018.06.052.

[44] B. P. Sobolev and N. L. Tkachenko, "Phase diagrams of BaF_2-(Y, Ln)F_3 systems," *J. Less Common Met.*, vol. 85, pp. 155–170, May 1982, doi: 10.1016/0022-5088(82)90067-4.

[45] A. de Pablos-Martín, A. Durán, and M. J. Pascual, "Nanocrystallisation in oxyfluoride systems: mechanisms of crystallisation and photonic properties," *Int. Mater. Rev.*, vol. 57, no. 3, pp. 165–186, May 2012, doi: 10.1179/1743280411Y.0000000004.

[46] G. Krieke, A. Sarakovskis, R. Ignatans, and J. Gabrusenoks, "Phase transitions and upconversion luminescence in oxyfluoride glass ceramics containing $Ba_4Gd_3F_{17}$ nanocrystals," *J. Eur. Ceram. Soc.*, vol. 37, no. 4, 2017, doi: 10.1016/j.jeurceramsoc.2016.12.023.

[47] A. De Pablos-Martín., D. Ristic, A. Durán, M. Ferrari, and M. J. Pascual, "Crystallization and optical properties of Tm^{3+}/Yb^{3+}-co-doped $KLaF_4$ glass-ceramics," *CrystEngComm*, vol. 19, no. 6, pp. 967–974, 2017, doi: 10.1039/c6ce01845a.

[48] A. de Pablos-Martín, M. O. Ramírez, a. Durán, L. E. Bausá, and M. J. Pascual, "Tm^{3+} doped oxy-fluoride glass-ceramics containing $NaLaF_4$ nano-crystals," *Opt. Mater. (Amst).*, vol. 33, no. 2, pp. 180–185, Dec. 2010, doi: 10.1016/j.optmat.2010.08.004.

[49] A. Herrmann, M. Tylkowski, C. Bocker, and C. Rüssel, "Cubic and Hexagonal $NaGdF_4$ Crystals Precipitated from an Aluminosilicate Glass: Preparation and Luminescence Properties," *Chem. Mater.*, vol. 25, no. 14, pp. 2878–2884, Jul. 2013, doi: 10.1021/cm401454y.

[50] R. E. Thoma, H. Insley, and G. M. Hebert, "The Sodium Fluoride-Lanthanide Trifluoride Systems," *Inorg. Chem.*, vol. 5, no. 7, pp. 1222–1229, Jul. 1966, doi: 10.1021/ic50041a032.

[51] R. Hill, D. Wood, and M. Thomas, "Trimethylsilylation analysis of the silicate structure of fluoro-alumino-silicate glasses and the structural role of fluorine," *J. Mater. Sci.*, vol. 4, pp. 1767–1774, 1999.

[52] I. Gugov, M. Müller, and C. Rüssel, "Transparent oxyfluoride glass ceramics co-doped with Er^{3+} and Yb^{3+} – Crystallization and upconversion spectroscopy," *J. Solid State Chem.*, vol. 184, no. 5, pp. 1001–1007, May 2011, doi: 10.1016/j.jssc.2011.03.017.

[53] L. A. Bueno, Y. Messaddeq, F. A. Dias Filho, and S. J. L. Ribeiro, "Study of fluorine losses in oxyfluoride glasses," *J. Non. Cryst. Solids*, vol. 351, no. 52–54, pp. 3804–3808, 2005, doi: 10.1016/j.jnoncrysol.2005.10.007.

[54] W. Vogel, "Phase separation in glass," *J. Non. Cryst. Solids*, vol. 24, no. 1–3, pp. 170–214, 1977, doi: 10.1016_0022-3093(77)90093-x.

[55] C. Bocker, C. Rüssel, and I. Avramov, "Transparent nano crystalline glass-ceramics by interface controlled crystallization," *Int. J. Appl. Glas. Sci.*, vol. 4, pp. 174–181, 2013, doi: 10.1111/ijag.12033.

[56] G. Krieke, A. Sarakovskis, and M. Springis, "Upconversion luminescence of Er^{3+}/Yb^{3+} and their role in the stabilization of cubic $NaLaF_4$ nanocrystals in transparent oxyfluoride glass ceramics," *J. Non. Cryst. Solids*, no. November, pp. 0–1, 2017, doi: 10.1016/j.jnoncrysol.2017.11.016.

[57] G. Gorni *et al.*, "Crystallization mechanism in sol-gel oxyfluoride glass-ceramics," *J. Non. Cryst. Solids*, vol. 501, no. December 2017, pp. 145–152, 2018, doi: 10.1016/j.jnoncrysol.2018.01.031.

[58] Y. Yu, Y. Wang, D. Chen, and F. Liu, "Efficient upconversion luminescence of $Er^{3+}:SrF_2$-SiO_2-Al_2O_3 sol-gel glass ceramics," *Ceram. Int.*, vol. 34, no. 8, pp. 2143–2146, Dec. 2008, doi: 10.1016/j.ceramint.2007.08.001.

[59] K. Kajihara, "Recent advances in sol-gel synthesis of monolithic silica and silica-based glasses," *J. Asian Ceram. Soc.*, vol. 1, no. 2, pp. 121–133, 2013, doi: 10.1016/j.jascer.2013.04.002.

[60] ASTM and C169-16, "Standard Test Methods for Chemical Analysis of Soda-Lime and Borosilicate Glass," 2016. .

[61] N. Kayal and N. Singh, "New Approach for the Determination of Fluorine in Glass," *Eurasian J. Anal. Chem.*, vol. 2, no. 3, 2007.

[62] Q. Mao *et al.*, "Broadband NIR emission from transparent fluorosilicate glass-ceramics containing $Rb_2SiF_6:Ni^{2+}$ nanocrystals," *J. Non. Cryst. Solids*, vol. 518, no. May, pp. 66–69, 2019, doi: 10.1016/j.jnoncrysol.2019.05.019.

[63] M. Walas *et al.*, "From structure to luminescence investigation of oxyfluoride transparent glasses and glass-ceramics doped with Eu^{3+}/Dy^{3+} ions," *J. Alloys Compd.*, vol. 806, pp. 1410–1418, 2019, doi: 10.1016/j.jallcom.2019.07.017.

[64] V. Marghussian, "Optical Properties of Nano-Glass Ceramics," in *Nano-Glass Ceramics*, Elsevier, 2015, pp. 63–123.

[65] J. I. Langford and A. J. C. Wilson, "Scherrer after sixty years: A survey and some new results in the determination of crystallite size," *J. Appl. Crystallogr.*, vol. 11, no. 2, pp. 102–113, Apr. 1978, doi: 10.1107/S0021889878012844.

[66] L. F. Vendramim, K. Zorn, C. Bocker, and C. Rüssel, "Effect of the alkali concentration on the crystallization of BaF_2 from $Na_2O/K_2O/BaF_2/Al_2O_3/SiO_2$ glasses," *J. Non. Cryst. Solids*, vol. 356, pp. 2999–3003, 2010, doi: 10.1016/j.jnoncrysol.2010.02.024.

[67] P. P. Fedorov, A. A. Luginina, and A. I. Popov, "Transparent oxyfluoride glass ceramics," *J. Fluor. Chem.*, vol. 172, pp. 22–50, 2015, doi: 10.1016/j.jfluchem.2015.01.009.

[68] G. Krieke, A. Sarakovskis, and M. Springis, "Upconversion luminescence of $Er^{3+}/Yb^{3+}$and their role in the stabilization of cubic $NaLaF_4$ nanocrystals in transparent oxyfluoride glass ceramics," *J. Non. Cryst. Solids*, 2017, doi: 10.1016/j.jnoncrysol.2017.11.016.

[69] K. J. J. Rao, *Structural chemistry of glasses*. 2002.

[70] M. Środa, C. Paluszkiewicz, M. Reben, and B. Handke, "Spectroscopic study of nanocrystallization of oxyfluoride glasses," *J. Mol. Struct.*, vol. 744–747, pp. 647–651, Jun. 2005, doi: 10.1016/j.molstruc.2004.11.079.

[71] M. Mattarelli *et al.*, "Tm³⁺-activated transparent oxy-fluoride glass-ceramics: Structural and spectroscopic properties," *J. Non. Cryst. Solids*, vol. 345–346, pp. 354–358, 2004, doi: 10.1016/j.jnoncrysol.2004.08.043.

[72] G. C. Righini and M. Ferrari, "Photoluminescence of rare-earth-doped glasses," *Riv. del Nuovo Cim.*, vol. 28, no. 12, pp. 1–53, 2005, doi: 10.1393/ncr/i2006-10010-8.

[73] Z. Zhou, W. Li, J. Song, B. Mei, G. Yi, and Y. Yang, "Application of Judd–Ofelt theory in analyzing Nd³⁺ doped SrF₂ and CaF₂ transparent ceramics," *J. Eur. Ceram. Soc.*, vol. 39, no. 7, pp. 2446–2452, 2019, doi: 10.1016/j.jeurceramsoc.2019.02.033.

[74] A. Polman, "Erbium as a probe of everything?," *Phys. B Condens. Matter*, vol. 300, no. 1–4, pp. 78–90, Jul. 2001, doi: 10.1016/S0921-4526(01)00573-7.

[75] K. M. Cirillo-Penn and J. C. Wright, "Laser spectroscopic measurement of point-defect dynamics in Eu³⁺:CaF₂," *Phys. Rev. B*, vol. 41, no. 15, pp. 10799–10807, 1990, doi: 10.1103/PhysRevB.41.10799.

[76] A. Antuzevics, G. Krieke, E. Pavlovska, and U. Rogulis, "Eu³⁺ ion distribution in oxyfluoride glass nanocomposites," *J. Non. Cryst. Solids*, vol. 522, no. May, 2019, doi: 10.1016/j.jnoncrysol.2019.119548.

[77] A. Sarakovskis, J. Grube, G. Doke, and M. Springis, "Excited state absorption and energy-transfer mechanisms of up-conversion luminescence in Er³⁺-doped oxyfluoride glass ceramics at different temperatures," *J. Lumin.*, vol. 130, no. 5, pp. 805–811, 2010, doi: 10.1016/j.jlumin.2009.11.037.

[78] I. V. Veksler, A. M. Dorfman, M. Kamenetsky, P. Dulski, and D. B. Dingwell, "Partitioning of lanthanides and Y between immiscible silicate and fluoride melts, fluorite and cryolite and the origin of the lanthanide tetrad effect in igneous rocks," *Geochim. Cosmochim. Acta*, vol. 69, no. 11, pp. 2847–2860, Jun. 2005, doi: 10.1016/j.gca.2004.08.007.

[79] G. Krieke and A. Sarakovskis, "Crystallization and upconversion luminescence of distorted fluorite nanocrystals in Ba²⁺ containing oxyfluoride glass ceramics," *J. Eur. Ceram. Soc.*, vol. 36, no. 7, pp. 1715–1722, Jun. 2016, doi: 10.1016/j.jeurceramsoc.2016.01.025.

[80] X. Qiao, X. Fan, Z. Xue, X. Xu, and Q. Luo, "Intense ultraviolet upconversion luminescence of Yb³⁺ and Tb³⁺ co-doped glass ceramics containing SrF₂ nanocrystals," *J. Lumin.*, vol. 131, no. 10, pp. 2036–2041, 2011, doi: 10.1016/j.jlumin.2011.05.012.

[81] A. de Pablos-Martin, C. Patzig, T. Höche, A. Duran, and M. J. Pascual, "Distribution of thulium in Tm³⁺-doped oxyfluoride glasses and glass-ceramics," *CrystEngComm*, vol. 15, no. 35, pp. 6979–6985, 2013, doi: 10.1039/c3ce40731d.

[82] N. Hu, H. Yu, M. Zhang, P. Zhang, Y. Wang, and L. Zhao, "The tetragonal structure of nanocrystals in rare-earth doped oxyfluoride glass ceramics.," *Phys. Chem. Chem. Phys.*, vol. 13, no. 4, pp. 1499–1505, 2011, doi: 10.1039/c0cp00903b.

[83] F. Liu, Y. Wang, D. Chen, and Y. Yu, "Investigation on crystallization kinetics and microstructure of novel transparent glass ceramics containing Nd:NaYF₄ nano-crystals," *Mater. Sci. Eng. B*, vol. 136, no. 2–3, pp. 106–110, Jan. 2007, doi: 10.1016/j.mseb.2006.09.012.

[84] M. Mattarelli *et al.*, "Tm³⁺-activated transparent oxy-fluoride glass-ceramics: Structural and spectroscopic properties," *J. Non. Cryst. Solids*, vol. 345–346, pp. 354–358, 2004, doi: 10.1016/j.jnoncrysol.2004.08.043.

[85] S. González-Pérez *et al.*, "Energy transfer in Pr³⁺–Yb³⁺ codoped oxyfluoride glass ceramics," *Opt. Mater. (Amst).*, vol. 29, no. 10, pp. 1231–1235, Jun. 2007, doi: 10.1016/j.optmat.2006.02.022.

[86] F. Lahoz, I. R. Martín, J. Méndez-Ramos, and P. Núñez, "Dopant distribution in a Tm³⁺-Yb³⁺ codoped silica based glass ceramic: An infrared-laser induced upconversion study," *J. Chem. Phys.*, vol. 120, no. 13, pp. 6180–6190, 2004, doi: 10.1063/1.1652016.

[87] R. Wang, X. Zhang, F. Liu, L. Xiao, Y. Chen, and L. Liu, "Upconversion mechanisms of Er³⁺:NaYF₄ and thermal effects induced by incident photon on the green luminescence," *J. Lumin.*, vol. 175, pp. 35–43, Jul. 2016, doi: 10.1016/j.jlumin.2016.02.018.

[88] S. S. T. Tatsuya, "Transparent crystallized glass," JP2014091650A, 2014.

[89] O. Yuhu and J. Wang, "A wavelength up-conversion glass ceramic and a process for the production thereof," EP0640571A1, 1995.

[90] S. Kang *et al.*, "Precisely controllable fabrication of Er³⁺-doped glass ceramic fibers: Novel mid-infrared fiber laser materials," *J. Mater. Chem. C*, vol. 5, no. 18, pp. 4549–4556, 2017, doi: 10.1039/c7tc00988g.

[91] C. Koepke, K. Wisniewski, M. Żelechower, and E. Czerska, "The role of phonons in the luminescence characteristics of SICLOF oxyfluoride glass and glass-ceramic fibers doped with Er³⁺/Yb³⁺," *J. Lumin.*, vol. 204, no. August, pp. 278–283, 2018, doi: 10.1016/j.jlumin.2018.08.035.

[92] T. Komatsu, "Design and control of crystallization in oxide glasses," *J. Non. Cryst. Solids*, vol. 428, pp. 156–175, 2015, doi: 10.1016/j.jnoncrysol.2015.08.017.

[93] K. Shinozaki, A. Noji, T. Honma, and T. Komatsu, "Morphology and photo-luminescence properties of Er3+-doped CaF2 nanocrystals patterned by laser irradiation in oxyfluoride glasses," *J. Fluor. Chem.*, vol. 145, pp. 81–87, 2013, doi: 10.1016/j.jfluchem.2012.10.007.

[94] S. D. Melgaard, A. R. Albrecht, M. P. Hehlen, and M. Sheik-Bahae, "Solid-state optical refrigeration to sub-100 Kelvin regime," *Sci. Rep.*, vol. 6, pp. 2–7, 2016, doi: 10.1038/srep20380.

[95] J. Zhong *et al.*, "A review on nanostructured glass ceramics for promising application in optical thermometry," *J. Alloys Compd.*, vol. 763, pp. 34–48, 2018, doi: 10.1016/j.jallcom.2018.05.348.

[96] G. Lee *et al.*, "Synthesis and Luminescence Properties of Transparent Nanocrystalline GdF₃:Tb Glass-Ceramic Scintillator.," *J. Lumin.*, vol. 147, pp. 363–366, Mar. 2014, doi: 10.1016/j.jlumin.2013.11.073.

[97] J. Cao, W. Chen, L. Chen, X. Sun, and H. Guo, "Synthesis and characterization of BaLuF₅: Tb³⁺ oxyfluoride glass ceramics as nanocomposite scintillator for X-ray imaging," *Ceram. Int.*, vol. 42, no. 15, pp. 17834–17838, 2016, doi: 10.1016/j.ceramint.2016.08.114.

[98] W. Chen *et al.*, "Highly efficient Na₅Gd₉F₃₂:Tb³⁺ glass ceramic as nanocomposite scintillator for X-ray imaging," *Opt. Mater. Express*, vol. 8, no. 1, p. 41, Jan. 2018, doi: 10.1364/OME.8.000041.

[99] E. Elsts *et al.*, "Studies of radiation defects in cerium, europium and terbium activated oxyfluoride glasses and glass ceramics," *Opt. Mater. (Amst).*, vol. 41, pp. 90–93, 2015, doi: 10.1016/j.optmat.2014.10.042.

[100] Z. Wang and L. Cheng, "Gamma ray irradiation-induced variations in structure and optical properties of cerium/titanium-doped oxyfluoride transparent glass-ceramics," *Mater. Res. Bull.*, vol. 92, pp. 104–112, 2017, doi: 10.1016/j.materresbull.2017.04.010.

[101] G. Okada *et al.*, "Samarium-doped oxyfluoride glass-ceramic as a new fast erasable dosimetric detector material for microbeam radiation cancer therapy applications at the canadian synchrotron," *J. Am. Ceram. Soc.*, vol. 97, no. 7, pp. 2147–2153, 2014, doi: 10.1111/jace.12938.

[102] M. Sheik-Bahae and R. I. Epstein, "Optical refrigeration," *Nat. Photonics*, vol. 1, no. 12, pp. 693–699, 2007, doi: 10.1038/nphoton.2007.244.

[103] G. Nemova and R. Kashyap, "Laser cooling with Tm^{3+}-doped oxy-fluoride glass ceramic," *J. Opt. Soc. Am. B*, vol. 29, no. 11, p. 3034, 2012, doi: 10.1364/josab.29.003034.

[104] K. V. Krishnaiah, E. Soares de Lima Filho, Y. Ledemi, G. Nemova, Y. Messaddeq, and R. Kashyap, "Development of ytterbium-doped oxyfluoride glasses for laser cooling applications," *Sci. Rep.*, vol. 6, no. 1, p. 21905, Apr. 2016, doi: 10.1038/srep21905.

[105] A. Khare, *A critical review on the efficiency improvement of upconversion assisted solar cells*, vol. 821. Elsevier B.V., 2020.

[106] H. Fu *et al.*, "Tunable white light emission from glass-ceramics containing Eu^{2+}, Tb^{3+}, Eu^{3+} co-doped $SrLaF_5$ nanocrystals," *Mater. Lett.*, vol. 71, pp. 15–17, Mar. 2012, doi: 10.1016/j.matlet.2011.12.004.

[107] Y. Ledemi *et al.*, "White light and multicolor emission tuning in triply doped Y^{3+}/Tm^{3+}/Er^{3+} novel fluoro-phosphate transparent glass-ceramics," *J. Mater. Chem. C*, vol. 2, no. 25, pp. 5046–5056, 2014, doi: 10.1039/C4TC00455H.

[108] Z. Chen *et al.*, "Near-infrared wavelength-dependent nonlinear transmittance tailoring in glass ceramics containing Er^{3+} :LaF_3 nanocrystals," *J. Mater. Chem. C*, vol. 4, no. 28, pp. 6707–6712, 2016, doi: 10.1039/C6TC01876A.

[109] J. Méndez-ramos, J. C. Ruiz-morales, and P. Acosta-mora, "Rare-earth doped nano-glass-ceramics for extending spectral response of water-splitting semiconductor electrodes by high intense UV-blue up-conversion : Turning the sun into blue," *J. Power Sources*, vol. 238, pp. 313–317, 2013, doi: 10.1016/j.jpowsour.2013.03.068.

[110] N. Doebelin and R. Kleeberg, "Profex : a graphical user interface for the Rietveld refinement program BGMN," *J. Appl. Crystallogr.*, vol. 48, no. 5, pp. 1573–1580, Oct. 2015, doi: 10.1107/S1600576715014685.

[111] K. Momma and F. Izumi, "VESTA 3 for three-dimensional visualization of crystal, volumetric and morphology data," *J. Appl. Crystallogr.*, vol. 44, no. 6, pp. 1272–1276, Dec. 2011, doi: 10.1107/S0021889811038970.

[112] R. E. Thoma, G. M. Hebert, H. Insley, and C. F. Weaver, "Phase Equilibria in the System Sodium Fluoride-Yttrium Fluoride," *Inorg. Chem.*, vol. 2, no. 5, pp. 1005–1012, Oct. 1963, doi: 10.1021/ic50009a030.

[113] D. Zakaria, R. Mahiou, D. Avignant, and M. Zahir, "Single-crystal structure refinement and luminescence analysis of β-$NaEuF_4$," *J. Alloys Compd.*, vol. 257, no. 1–2, pp. 65–68, Jul. 1997, doi: 10.1016/S0925-8388(97)00016-9.

[114] A. Sarakovskis, G. Krieke, G. Doke, J. Grube, L. Grinberga, and M. Springis, "Comprehensive study on different crystal field environments in highly efficient $NaLaF_4 : Er^{3+}$ upconversion phosphor," *Opt. Mater. (Amst).*, vol. 39, pp. 90–96, Jan. 2015, doi: 10.1016/j.optmat.2014.11.004.

[115] M. Pollnau, D. R. Gamelin, S. R. Lüthi, H. U. Güdel, and M. P. Hehlen, "Power dependence of upconversion luminescence in lanthanide and transition-metal-ion systems," *Phys. Rev. B*, vol. 61, no. 5, pp. 3337–3346, Feb. 2000, doi: 10.1103/PhysRevB.61.3337.

[116] G. Krieke, A. Sarakovskis, and M. Springis, "Cubic and rhombohedral $Ba_4Lu_3F_{17}$:Er^{3+} in transparent glass ceramics: Crystallization and upconversion luminescence," *J. Lumin.*, vol. 200, pp. 265–273, 2018, doi: 10.1016/j.jlumin.2018.04.016.

[117] I. V. Veksler *et al.*, "Partitioning of elements between silicate melt and immiscible fluoride, chloride, carbonate, phosphate and sulfate melts, with implications to the origin of natrocarbonatite," *Geochim. Cosmochim. Acta*, vol. 79, pp. 20–40, Feb. 2012, doi: 10.1016/j.gca.2011.11.035.

[118] B. A. Maksimov *et al.*, "The fluorite-matrix-based $Ba_4R_3F_{17}$ (R = Y, Yb) crystal structure. Ordering of cations and specific features of the anionic motif," *Crystallogr. REPORTS*, vol. 41, no. 1, pp. 50–57, 1996.

[119] B. P. Sobolev *et al.*, "$Ba_{1-x}R_xF_{2+x}$ Phases (R = Gd-Lu) with distorted fluorite-type structures—products of crystallization of incongruent melts in the BaF_2-RF_3 Systems (R = Gd-Lu). III. Defect $Ba_{0.75}Lu_{0.25}F_{2.25}$ structure. A new $\{Lu_8[Ba_6F_{71}]\}$ supercluster of defects," *Crystallogr. Reports*, vol. 48, no. 6, pp. 944–952, Nov. 2003, doi: 10.1134/1.1627436.

ACKNOWLEDGEMENTS

I wish to express gratitude to my supervisor Anatolijs Sarakovskis for support and lengthy discussions which helped me to find solutions to many challenges in glass ceramic research.

I wish to thank the staff of UL ISSP, who assisted during the preparation of these thesis and taught me both theory and practical aspects of luminescence spectroscopy. Especial thanks to Maris Springis, who offered invaluable discussions about wide variety of topics from fundamentals of spectroscopy to practical aspects of solid state mechanics, Uldis Rogulis for detailed explanation about the formation and analysis methods of intrinsic defects, Jurgis Grube and Guna Doke for assistance with the spectroscopic measurements, Meldra Kemere and Andris Antuzevics for close collaboration and regular inquiries about progress of theses, Jevgenijs Gabrusenoks for Raman measurements which allowed the interpretation of the origin of high luminescence efficiency of $Ba_4RE_3F_{17}$, Krisjanis Smits for TEM measurements which were indispensable for analysis of individual nanoparticles, Karlis Kundzins for tutoring me on SEM measurements and Reinis Ignatans for inspiring discussions and Rietveld refinement of crystal structures.

In addition, I want to express gratitude to my family who supported my thorough my studies, especially Romans without whom these theses would have been completed at least a year earlier.